December 16, 1968

To the Graduate Council:

I am submitting herewith a dissertation written by Richard Carl Hagenauer, entitled "The Decay of Neutron Deficient Nuclides of Mass 89." I recommend that it be accepted in partial fulfillment of the requirements for the degree of Doctor of Philosophy, with a major in Chemistry.

J. Davis O'Kelley
Major Professor

We have read this dissertation and recommend its acceptance:

Geo. K. Schweitzer

William E Bull

Robert W. Lide

Accepted for the Council:

Hilton A. Smith
Vice Chancellor for
Graduate Studies and Research

THE DECAY OF NEUTRON DEFICIENT NUCLIDES OF MASS 89

A Dissertation

Presented to

the Graduate Council of

The University of Tennessee

In Partial Fulfillment

of the Requirements for the Degree

Doctor of Philosophy

---

by

Richard Carl Hagenauer

March 1969

ACKNOWLEDGMENT

The author would like to thank Drs. G. Davis O'Kelley and Eugene Eichler for their research direction and assistance, including many long hours of data acquisition. Their assistance and advice have made his stay at Oak Ridge an invaluable experience. The courses in Nuclear Chemistry, well taught by Dr. G. Davis O'Kelley, were indispensable for this research.

The help of the staff of the Chemistry Division of Oak Ridge National Laboratory is gratefully acknowledged. In particular, the author would like to thank Dr. E. H. Taylor, Director of the Chemistry Division, for use of the Division's facilities. The author is grateful to Mrs. Jeane Fullerton for her accurate typing, and to Mr. William Dunlap for drawing most of the figures used in this dissertation. The author is also indebted to Mr. A. W. Riikola and the crew of the Oak Ridge Isochronous Cyclotron for experimental help and beam development. The computer-programming assistance given by Mr. Richard Kuebbing, Mr. Ronald McCann, and Mr. Alton Jenkins is greatly appreciated.

The author is indebted to Oak Ridge Associated Universities for its financial support in the form of an Oak Ridge Graduate Fellowship. This research was carried out in the Chemistry Division of the Oak Ridge National Laboratory, sponsored by the U. S. Atomic Energy Commission under contract with Union Carbide Corporation.

861563

ABSTRACT

The decays of 78-hr ^{89}Zr and 4-min $^{89}Zr^{m}$ have been investigated using Ge(Li) γ-ray detectors. It was established that decay of 78-hr ^{89}Zr populates the levels at 909.2, 1744.5, 2530.0, 2566.5, and 2622.1 keV in ^{89}Y; and the decay of 4-min $^{89}Zr^{m}$ populates the level at 1507.4 keV in ^{89}Y. The spin assignments have been made from log *ft* values and previously reported data from studies of nuclear reactions. The half-lives of ^{89}Zr and $^{89}Zr^{m}$ have been measured to be 78.0 ± 0.2 hr and 4.16 ± 0.06 min, respectively. The levels of ^{89}Y are compared with previously reported levels determined from nuclear reaction studies.

The decays of 112-min ^{89}Nb and 66-min $^{89}Nb^{m}$ have been investigated using Ge(Li) and NaI(Tl) γ-ray and anthracene β-ray detectors. Coincidence relationships among the γ-rays were established in γ-γ coincidence experiments. The decay of ^{89}Nb populates levels at 588.8, 1095.5, 1451.8, 1512.2, 1627.8, 1865.6, 2102.0, 2129.0, 2299.5, 2573.5, 2613.1, 2754.6, 2890.5, 2926.4, 2961.1, 2983.5, 3017.4, 3093.5, 3467.0, 3513.3, 3557.8, 3576.3, 3839.1 and 3965.5 keV in ^{89}Zr. The decay of $^{89}Nb^{m}$ populates levels at 588.8, 1095.5, 1746.0, and 1865.6 keV in ^{89}Zr. Some spin assignments have been made from log *ft* values and the selection rules for gamma decay. The fraction of positron decay to the ground state was found to be 74 per cent. Three beta rays of energies 3.34 ± 0.10, 2.82 ± 0.12, and 2.38 ± 0.15 MeV have been measured with an anthracene detector. The half-lives of ^{89}Nb and $^{89}Nb^{m}$ were found to be 122 ± 4

min and 66 ± 2 min respectively. The levels of ^{89}Zr were compared with levels determined from nuclear reaction studies and shell model calculations.

A search for ^{89}Mo and $^{89}Mo^{m}$ was conducted with Ge(Li) detectors. Despite rapid chemistry no growth of ^{89}Nb and $^{89}Nb^{m}$ was observed. The upper limits for the half-lives of ^{89}Mo and $^{89}Mo^{m}$ are 43 sec and 24 sec respectively. The excitation function for the $^{92}Mo(p,p2n)^{90}Mo$ reaction was measured at energies from 25 to 62 MeV.

TABLE OF CONTENTS

CHAPTER		PAGE
I.	INTRODUCTION	1
	A. Shell Model	2
	1. Nucleon-Nucleon Coupling	5
	2. The Effective Interaction Method	10
	3. Explicit Two Body Force Method	10
	B. Decay Schemes	11
	1. Gamma Decay	11
	2. Beta Decay	13
	3. Nuclear-Reaction Spectroscopy	17
	C. Spectroscopy of the Mass-89 Region	18
II.	EXPERIMENTAL PROCEDURES	20
	A. Instrumentation	20
	1. Detectors	20
	2. Amplifying Systems	23
	3. Multichannel Analyzers	27
	4. Instruments for Timing	29
	5. Gamma-Gamma Coincidence Counting System	31
	6. Positron Scintillation Spectrometer	34
	B. Radiochemical Separations	36
	1. Molybdenum	36
	a. Procedure 1	36
	b. Procedure 2	37

CHAPTER PAGE

c. Procedure 3 38
d. Procedure 4 39
2. Niobium 43
3. Zirconium 43
C. Data Analysis 44
1. Program TAPE 44
2. Program KORRECT 45
3. Program DAZYMA 46
4. Program FYSREV 46
5. Program FRANTIC 46
6. Program KURIE 47
III. EXPERIMENTAL RESULTS 48
A. The Decays of Zirconium-89 and Zirconium-89m 48
1. Previous Work 48
2. Experimental Procedure 48
3. Decay Scheme 51
a. Ground State 51
b. The 909.1-keV Level 54
c. The 1507.4-keV Level 54
d. The 1744.5-keV Level 54
e. The 2622.1-, 2566.5-, and 2530.0-keV Levels . . . 55
f. The 2.86- and 3.09- MeV Levels 55
B. The Decays of Niobium-89 and Niobium-89m 55
1. Previous Work 55

CHAPTER PAGE

2. Gamma-Ray Singles Spectra 56
3. Gamma-Gamma Coincidence Measurements 63
4. Positron Measurements 63
5. Decay Scheme 70
1. General Remarks 70
2. Beta Transitions 74
3. The 587.8-keV Level 76
4. The 1095.5-keV Level 76
5. The 1746.0- and 1865.6-keV Levels 76
6. The 1451.8-keV Level 76
7. The 1834.1-keV Level 79
8. The 2754.6- and 3093.5-keV Levels 79
9. The 1627.8-keV Level 80
10. The 2961.4-keV Level 80
11. The 3017.4-keV Level 80
12. The 2573.5-keV Level 80
13. The 2129.0-keV Level 81
14. Half-lives 81
C. The Search for Molybdenum-89 and Molybdenum-89m 83
1. Previous Work 83
2. Isomer Predictions 83
3. Experimental Procedures 86
a. Chemical Search 86
b. Excitation Function 93

CHAPTER PAGE

c. Final Results 94

IV. CONCLUSION 98

BIBLIOGRAPHY 101

APPENDIX 105

VITA 111

LIST OF TABLES

TABLE		PAGE
I.	Selection Rules for Gamma Transition	12
II.	Selection Rules for Beta Transitions	15
III.	Summary of the Gamma-Ray Results of the ^{89}Zr Isomers	52
IV.	Summary of the $^{89}Nb^{m}$ Gamma-Ray Results	64
V.	Summary of the ^{89}Nb Gamma-Ray Results	65
VI.	Summary of Coincident Gamma Rays of ^{89}Nb and $^{89}Nb^{m}$ Determined in the NaI-Ge(Li) Coincidence Experiment	69
VII.	Values of log *ft* for Beta Transitions in the Decay of ^{89}Nb and $^{89}Nb^{m}$	77
VIII.	Summary of the Upper Limits for ^{89}Mo and $^{89}Mo^{m}$ Half-Lives Determined from the Four Different Chemical Procedures	92
IX.	Zirconium Products from the Bombardment of $^{90}ZrO_2$ with 62-MeV Protons	96

LIST OF FIGURES

FIGURE PAGE

1. Energies of Single-Particle Orbitals in Harmonic-Oscillator and Rounded Square-Well Potentials, the Latter with and without Spin-Orbit Coupling. Numbers in ( ) Indicate Orbital Capacities and Those in [ ] Give Cumulative Capacity through a Given Orbital 4

2. Schematic Representation of the Couplings of j^2 that Give Maximum and Minimum Overlap. At the Right Is Shown the Relative Lowering of the Energy of the Configuration for Couplings to Various J values. The Top Line Shows the Position of All the Couplings When the Coupling Force is "Turned Off" 8

3. Pulse Shaping Circuits Used in the TC-200 Amplifier . . . 26

4. Block Diagram of Electronic System Used in the Ge(Li)-NaI Coincidence Experiments 32

5. Block Diagram of Electronic System Used to Measure Positrons 35

6. Over-All View of the Cyclotron Beam Pipe Showing the Molybdenum Separation Apparatus in Relation to the Magnetic Quadrupole Lens 40

FIGURE PAGE

7. Close-Up View of the Automatic Chemistry System for Molybdenum Separations 41

8. Sketch of Chemical Equipment in the Photograph of Figure 7, Showing Schematically the Flow of Chemical Reagents in the Molybdenum Separation 42

9. A Gamma-Ray Spectrum of ^{89}Zr Taken with a 20 cm^3 Ge(Li) Detector 50

10. The Decay Scheme Proposed for ^{89}Zr and $^{89}Zr^m$. Levels Determined by Hinrichsen, Shafroth, and Van Patter from $^{89}Y(p,p')$ Reaction Work Are Shown for Comparison. Positron and Electron Capture Branches Not in Parenthesis Were Measured Directly by Van Patter and Shafroth 53

11. The Low-Energy Portion of the ^{89}Nb Gamma Ray Spectrum Taken With a 35 cm^3 Ge(Li) Detector. The Spectrum in Part (a) Was Not Counted through Lead. The Spectrum in Part (b) Was Counted Through 1.5 cm of Lead 58

12. The High-Energy Portion of the ^{89}Nb Gamma Ray Spectrum Taken with a 35 cm^3 Ge(Li) Detector by Counting Through 1.5 cm^3 of Lead. Energies are in keV. Single and Double Escape Peaks are Represented Respectively as SE and DE 59

13. The Growth and Decay of the 588-keV Gamma-Ray Counted 2 Minutes after a Zirconium Separation 60

FIGURE PAGE

14. The Decay of the 1129-keV Gamma-Ray Showing ^{90}Nb and ^{89}Nb Components 62

15. Gamma-Ray Spectrum (NaI) of ^{89}Nb in Coincidence with Gamma Rays Counted with a Ge(Li) Detector 68

16. Fermi Analysis of the Positron Spectrum of ^{89}Nb and ^{89}Nb^{m} 71

17. Decay Scheme Proposed for ^{89}Nb and ^{89}Nb^{m} 72

18. A Comparison of the Experimental Level Spectra Obtained from the Decay of the ^{89}Nb Isomers, the ^{90}Zr(p,d) Reaction, and the Results of the Effective Interaction Method Obtained by Ball 82

19. Schematic Shell-Model Description of (a) Ground State of ^{89}Mo, and (b) ^{89}Mo^{m} 85

20. Excitation Function for ^{92}Mo(p,p2n) ^{90}Mo 95

CHAPTER I

INTRODUCTION

The properties of nuclei are largely determined by the forces between nucleons. These forces can not be determined directly; instead, a model can be formulated based on assumed nuclear forces. The success or failure of the model depends on its ability to account for observed nuclear properties. The model described in this thesis and used to interpret the experimental results is the shell model[1] modified by the "effective interaction" method.

The nuclear force is very strong and of very short range. If two nucleons pass within about 2×10^{-13} cm from each other, a very strong attractive force will bind these particles together. This force becomes repulsive if they approach a distance of about 0.4×10^{-13} cm. At large distances the electrostatic Coulomb force causes protons to repel each other. Since neutrons have no electrical charge, there is no long-range repulsion between neutrons or between a proton and neutron. In a nucleus containing many nucleons, each nucleon is affected by the short- and long-range forces of all the other nucleons. The sum of these short-range forces can be replaced by a central potential field. In this treatment the potential energy acting on one nucleon is a function of the nucleon coordinates but does not depend upon coordinates of the other nucleons.

A. SHELL MODEL

Theorists have found that for a spherical nucleus, the three-dimensional harmonic oscillator provides a good starting point for calculations of the nuclear potential. The equation for a harmonic oscillator in two dimensions is:

$$V(r) = - V_o \left[1 - \left(\frac{r}{R}\right)^2\right] .$$

In this expression R is the nuclear radius, r is the distance along the x axis and V_o is the potential r = 0. To determine the energy levels one must solve the Schrödinger equation,

$$\left(- \frac{\hbar^2}{2M} \nabla^2 + V(r)\right)\psi = \varepsilon\psi ,$$

where M is the nuclear mass. The solution gives rise to eigenvalues ε given by:

$$\varepsilon = \hbar\omega[2(n - 1) + \ell] , \qquad (1)$$

where ω is the oscillator frequency, and n and ℓ are radial and orbital momentum quantum numbers. The oscillator frequency is given by

$$\omega = \sqrt{\frac{2V_o}{MR^2}} .$$

As in atomic spectroscopy, levels with angular momentum ℓ = 0, 1, 2, 3, 4 ... are designated s, p, d, f, g .... Equation 1 yields energy levels with much degeneracy. The ground state, 1s, corresponds to n = 1, ℓ = 0. The next excited state 1p corresponds to n = 1, ℓ = 1. The 2s level is degenerate with the 1d level, since the quantum numbers n = 2,

$\ell = 0$ will give the same ε as $n = 1$ $\ell = 2$. Each additional shell may likewise contain several degenerate levels. This degeneracy may be removed by adding a square-well modification[2] which changes the shape of the potential as shown in the upper part of Figure 1.

A nuclear potential of this type is that of Woods and Saxon,[4] whose square well with rounded edges is given by

$$V(r) = - \frac{V_o}{1+e^{\alpha(r-R)}} ,$$

where α is a shape factor.

Another force which contributes greatly to the ordering of levels arises from spin-orbit coupling. The intrinsic nuclear spin s couples with the orbital angular momentum forming a new state with a quantum number j. A parallel coupling of s to ℓ gives rise to j where $j = s + \ell$. This state lies much lower in energy than the antiparallel coupling of s to ℓ where $j = s - \ell$. Now the nuclear potential can be calculated as follows:

$$V = V(r) + f(r) \cdot (\vec{s} - \vec{\ell}) ,$$

where $f(r)$ is a radial function dependent on the quantum number n. Both quantum numbers n and ℓ determine how great will be the splitting between the two levels. Figure 1 shows how these modifications affect the energy levels. The energy levels for protons and neutrons are similar, except proton levels generally lie at higher energy and have greater spin-orbit splitting from the Coulomb effect.

A given level will hold $2j + 1$ nucleons. The lower energy levels

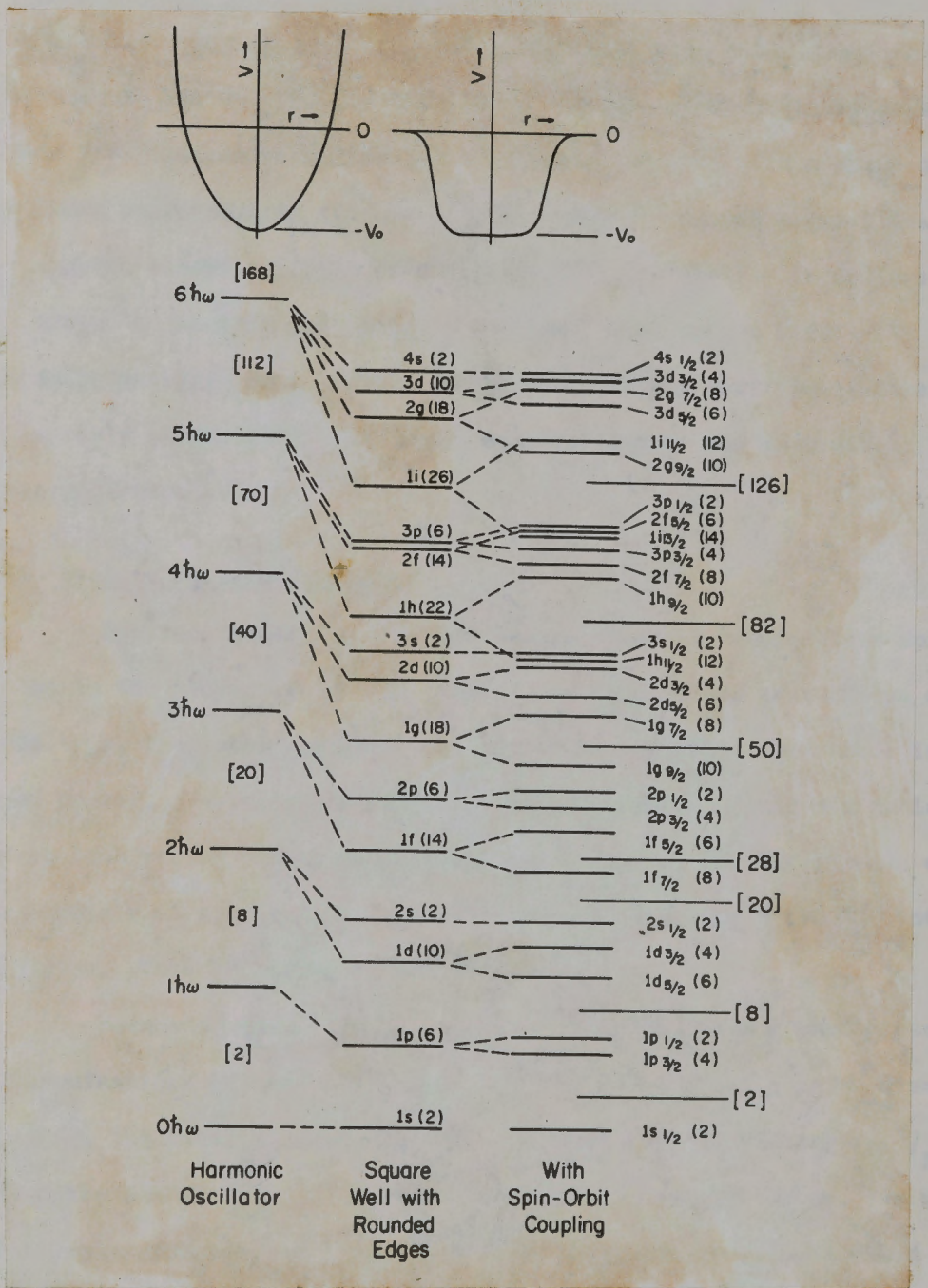


Figure 1. Energies of single-particle orbitals in harmonic-oscillator and rounded square-well potentials, the latter with and without spin-orbit coupling. Numbers in ( ) indicate orbital capacities and those in [ ] give cumulative capacity through a given orbital.[3]

fill first. Figure 1 shows large energy gaps when the nucleus is filled with 2, 8, 20, 28, 50, 82, and 126 protons or neutrons; these gaps indicate the presence of nuclear closed shells. Nuclei with neutron or proton numbers corresponding to these "magic numbers" require a great deal more energy to remove a proton or a neutron from the shell. It follows that a proton or neutron just outside the shell will have a relatively lower binding energy. Such binding-energy correlations contributed some of the early evidence for the "magic numbers" before the theoretical basis was understood.

1. Nucleon-Nucleon Coupling

Nucleons occupying the same orbital tend to couple their spins to zero in the ground state. If there is an even number of nucleons of one type, the total angular momentum $\vec{j}$ will be zero. When there is an odd number, $\vec{j}$ usually corresponds to the j orbital of the odd nucleon. When both proton and neutron numbers are odd, the j's for protons and neutrons will couple to give a total angular momentum J for the entire nucleus. This is called jj coupling.

Nordheim[5] has proposed the following method for ground-state determinations of odd-odd nuclei. If the sum of ℓ and j is an even number, the total angular momentum J is given by the difference $|j_p - j_n|$. When the sum of the ℓ and j quantum numbers is an odd number, the resultant spin approaches the sum of the j's, i.e., $|j_p + j_n|$. A third rule due to Brennan and Bernstein[6] involves "particle" and "hole" states. A "particle" state contains a subshell that is less than one-half full,

while a "hole" state involves a subshell that is half full or more. When a nucleus contains a neutron "hole" state and a proton "particle" state or vice versa, the resultant ground state spin is one less than the sum of the j's.

These three rules may be summarized as follows:

If $j_p + j_n + \ell_p + \ell_n$ = even number, then $J = |j_p - j_n|$.

If $j_p + j_n + \ell_p + \ell_n$ = odd number, then $J \leq |j_p + j_n|$.

For mixed particle-hole states, $J = j_{part.} + j_{hole} - 1$.

Several factors affect the coupling of nucleons to determine the excited state properties.

1. Overlap of the nucleon wave functions
2. Pairing energy
3. Details of the nucleon-nucleon coupling force

The tendency for nucleons to pair is an example of so-called "residual interactions." These are proton-proton (p-p), neutron-neutron (n-n), or proton-neutron (p-n) interactions of particles outside the closed shell. The first particle to occupy an orbital is given a spin of j. In the ground state the second particle will have a spin of $-j$. Thus the wave functions of the two nucleons have maximum overlap and an angular momentum of zero. However, in the excited state the $\vec{j}$ of the second nucleon may be found at some angle other than 180° from the $\vec{j}$ of first nucleons. There will be less overlap of the wave functions, which corresponds to a higher energy. When the $\vec{j}$'s are perpendicular there will be a minimum of overlap. The total angular momentum is a resultant of the two vectors. When perpendicular, the resultant spin J is

approximately equal to $j\sqrt{2}$. Other possible spins vary by two units from the maximum value of J allowed to zero for particles of the same orbital. For example, two neutrons in a $g_{9/2}$ level may couple five different ways to give J values of 0, 2, 4, 6 and 8, as shown in Figure 2. This is an example of the first effect. For odd-odd nuclei the levels may be mixed. There are $(2j_a + 1)$ ways in which these two particles can couple, where j_a is the spin of the particle of lower j. In odd-A nuclei, excited states may correspond to a coupling of the odd particle to another nucleon pair. For example, a spin of 21/2, corresponding to a $d_{5/2}$ neutron coupled to a $J = 8$ proton configuration, has been predicted and found[7] in ^{93}Mo.

The parity of a system is dependent on the symmetry properties of the wave function which describes the state. If the wave function for a system changes sign when the signs of all the space coordinates are changed it is said to have odd parity. If the sign of the wave function does not change it is said to have even parity. Parity is connected with the angular-momentum quantum number ℓ. States with even ℓ (s,d,g... states) have even parity, while those with odd ℓ (p,f,h... states) have odd parity. Two particles in states of even parity or two particles in states of odd parity can combine to a state of even parity only. A particle of even parity and one of odd parity couple to form a system of odd parity.

Another force which influences level order is due to pairing. For every pair of nucleons, the binding energy of the nucleus is increased by a pairing energy. The magnitude of this pairing energy

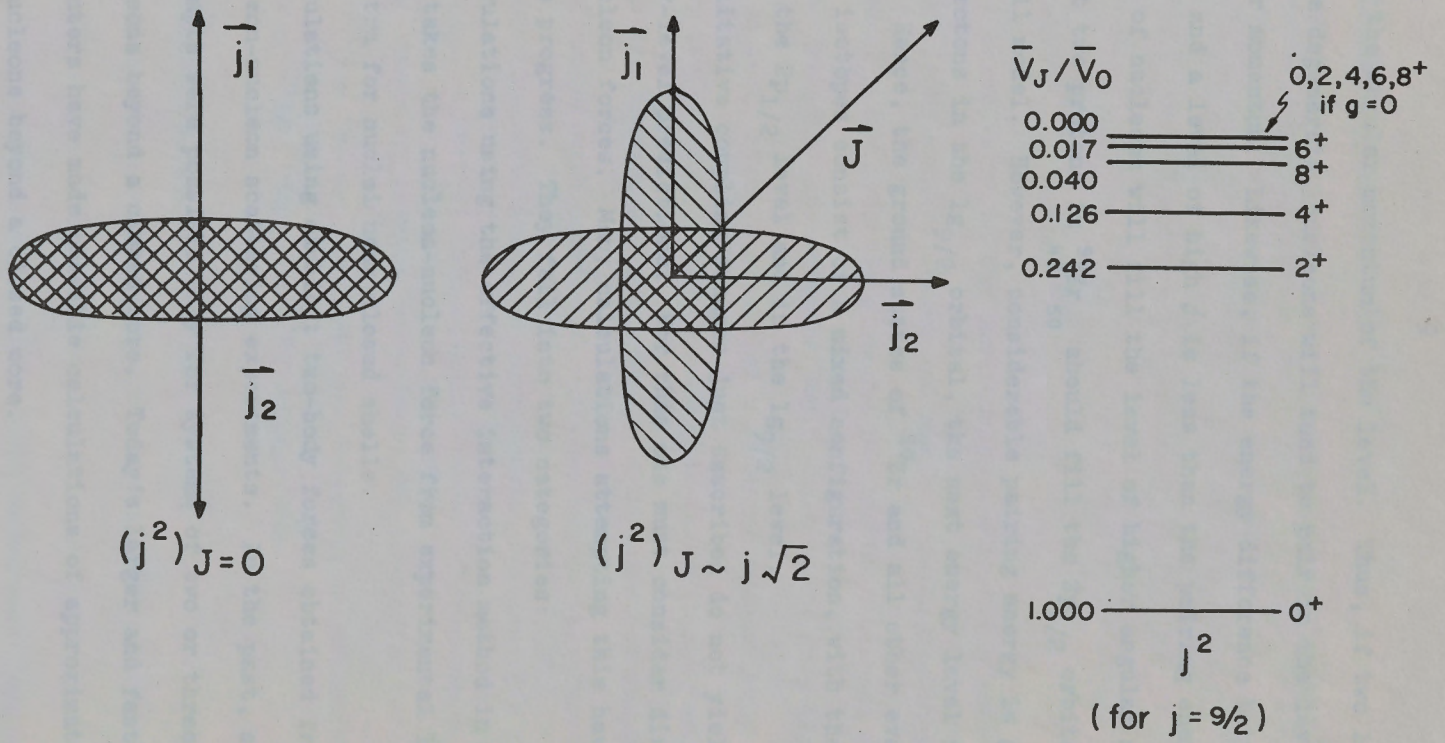


Figure 2. Schematic representation[3] of the couplings of j^2 that give maximum and minimum overlap. At the right is shown the relative lowering of the energy of the configuration for couplings to various J values. The top line shows the position of all the couplings when the coupling force is "turned off."

increases with the angular momentum of the level. Thus, if two levels of different j are degenerate, nucleons will tend to pair in the level of highest angular momentum. Likewise, if the energy difference between a level of low j and a level of high j is less than the pairing energy, the first pair of nucleons will fill the level of higher angular momentum.

The last two protons in $^{90}_{40}Zr_{50}$ should fill the $2p_{1/2}$ orbital in the simple shell model. However, considerable pairing energy is gained by a pair of protons in the $1g_{9/2}$ orbital, the next energy level in the filling order. Hence, the ground states of ^{90}Zr and all other even-even zirconium isotopes consist of a mixed configuration, with the last two protons in the $2p_{1/2}$ level and in the $1g_{9/2}$ level.

The qualitative coupling schemes just described do not yield explicit energy-level predictions. For this one must consider directly the nucleon-nucleon forces. Many calculations attempting this have been made and are in progress. They fall into two categories:

1. Calculations using the effective interaction method in which one takes the nucleon-nucleon force from experimental level spectra for nuclei near closed shells.
2. Calculations using explicit two-body forces obtained from nucleon-nucleon scattering experiments. In the past, such attempts were possible only for systems of two or three nucleons beyond a closed core. Today's larger and faster computers have made possible calculations of approximately 16 nucleons beyond a closed core.

2. The Effective Interaction Method

For calculations using the "effective interaction" method,[8] the Hamiltonian for the nucleus is written as:

$$H = H_{core} + \sum_{p} H_{p\text{-core}} + \sum_{n} H_{n\text{-core}} + \sum_{pairs} H_{p\text{-}p} + \sum_{pairs} H_{n\text{-}n} + \sum_{pairs} H_{p\text{-}n} .$$

The first three terms of the Hamiltonian contribute a constant energy to the low-lying excited states and can be considered the zero point of the energy scale. Matrix elements for the Hamiltonians of the p-p, n-n, and p-n residual interactions can be calculated from experimental results on level spectra of nuclei consisting respectively of a closed core plus two protons, a closed core plus two neutrons, and a closed core plus one neutron and one proton. With these desired potentials, levels of nuclei with additional nucleons beyond the closed core can be calculated. The consistency of experimental results with the predicted results is a test of this coupling scheme. For example, the low-lying energy levels of niobium, molybdenum and technetium have been calculated[9,10,11] from the n-n, p-p, and p-n interactions determined from the spectra of ^{92}Zr, ^{92}Mo, and ^{92}Nb respectively.

3. Explicit Two-Body Force Method

Other shell-model calculations use the absolute forces between nucleons to calculate excited states. The results of proton-scattering experiments on protons and neutrons, and neutron bombardments on neutrons give quantitative forces between the protons and neutrons.

B. DECAY SCHEMES

The diagram which shows the energy levels and spins of a nucleus as determined from the decay of the parent is called a decay scheme. There are selection rules for gamma and beta decay which are of great assistance in making assignments of spins and energies to nuclear levels.

1. Gamma Decay

Gamma rays are emitted when there is a shift of charge density or current density. A shift in charge density gives rise to a change in the electric moment. Gamma rays emitted from this process are called electric transitions and are designated as E. Likewise, a shift in current density gives rise to magnetic moments and the emitted gamma rays are designated as M. Electric transitions are much faster than magnetic transitions.

Gamma rays have an intrinsic spin of one and must carry away at least one unit of angular momentum. Transitions become slower when they must carry away more than one unit of angular momentum. Transitions carrying away ℓ units of angular momentum are designated as Mℓ or Eℓ transitions. Parity rules must also be followed. If the initial and final states have the same parity, only E transitions of even ℓ and M transitions of odd ℓ are allowed[12] (Table I). Most transitions observed in nuclei are E1, M1, and E2 gamma transitions, corresponding to spin changes of zero or one with or without a parity change, or two with no parity change. If a nucleus in the excited state has several possible levels to which it can decay, the fastest transitions

TABLE I

SELECTION RULES FOR GAMMA TRANSITIONS

Spin Change	Parity Change	Transition Type
0	No	M1
0	Yes	E1
1	No	M1
1	Yes	E1
2	No	E2
2	Yes	M2
3	No	M3
3	Yes	E3
4	No	E4
4	Yes	M4

will be more probable. Since electric multipole transitions are faster, Mℓ transitions will compete with E(ℓ + 1) transitions. The probability of a gamma-ray transition is also a function of energy: the higher the energy, the more favored the transition.

2. Beta Decay

In a similar manner, beta decay follows selection rules which are helpful in determining spins of energy levels. Positive and negative beta particle emission involves a simultaneous emission of an electron and a neutrino.

The probability for the emission of a beta particle[13] with momentum between η and $\eta + d\eta$ is given as

$$P(\eta)d\eta = G^2/2\pi^3|M|^2F(Z,\eta)\eta^2(\varepsilon_o - \varepsilon)\, d\eta\ , \qquad (2)$$

where η is the momentum of the electron in units of mc, $F(Z,\eta)$ is a Coulomb correction, ε is the total energy in units of m_oc^2, and ε_o is the maximum energy of the beta distribution. The quantity $(\varepsilon_o - \varepsilon)$ represents the momentum and energy of the neutrino. The factor G is proportional to the strength of the interaction between the nucleons and the electron-neutrino field. The factor $|M|^2$ represents the square of the matrix element containing the wave functions of the initial and final states of the neutron and proton and the form of the nuclear interaction. These states determine the angular momentum for the emitted electrons. The probability for emission of electrons will be much larger for *s*-wave electrons than for electrons of higher angular momentum. For these "allowed" transitions the electrons will carry away no angular momentum,

and $\Delta\ell$ between the initial and final states will be zero. Also the parities of the initial and final states must be the same. If the intrinsic spins of the electron and neutrino are aligned antiparallel, the spin change ΔI will be zero; if the spins are aligned parallel ΔI will be plus or minus one.

There is a finite probability of *p*-wave or *d*-wave electron emission, since the wave functions do not vanish at the nucleus. The probability decreases rapidly with increasing angular momentum. The beta transitions corresponding to angular momentum changes of ℓ = 1, 2, 3, and 4 are called first-, second-, third-, and fourth-forbidden, respectively. Changes in angular momentum which are even involve no parity changes, while odd-ℓ intervals do involve parity changes. The selection rules for beta decay are given in Table II.

Other factors which determine the speed of a beta transition are transition energy and atomic number of the nucleus. A large energy change between the initial and final states increases the probability of beta emission. The nuclear charge provides a Coulomb effect, which enhances positron emission and hinders negative beta decay slightly.

The decay constant for a transition is obtained by integrating the momentum probability distribution from zero to η_{max} as shown below:

$$\lambda = \frac{\ln 2}{t_{1/2}} = \int_0^{\eta_{max}} P(\eta)d\eta = G^2/2\pi^3|M|^2 f(Z,\varepsilon_o) \ ,$$

where

$$f(Z,\varepsilon_o) = \int_0^{\eta_{max}} F(Z,\eta)\ \eta^2\ (\varepsilon_o - \varepsilon)^2\ d\eta$$

TABLE II

SELECTION RULES FOR BETA DECAY

Transition Type	ℓ-Change	Spin Change	Parity Change	Average log *ft*
Allowed (favored)	0	0 or 1	No	3.5±0.2
Allowed (normal)	0	0 or 1	No	5.7±1.1
First forbidden	1	0 or 1	Yes	7.5±1.5
First forbidden (unique)	1	2	Yes	8.5±0.7
Second forbidden	2	2	No	12.1±1.0
Second forbidden (unique)	2	3	No	11.7±0.9

The product of $f(Z,\varepsilon_o)$ and $t_{1/2}$ in sec, denoted as *ft*, is a measure of the forbiddenness of a beta transition. Values of *ft* fall into groups in which each degree of forbiddenness increases by a factor of 100. Conventionally values of log *ft* are used to deduce the degree of forbiddenness of beta transition. Low values of log *ft* represent favored transitions, while larger values correspond to forbidden transitions. By measuring the log *ft* values one can infer the spin changes between the initial and final states of beta decay. The average values of log *ft* for various types of beta transitions[14] are included in Table II.

Any time positron emission is energetically possible, electron capture may compete. Electron capture is favored when the *Q* value (energy between initial and final states) is low. If the *Q* value is less than 1.022 MeV, the decay will be entirely by electron capture. Values of log *ft* for electron capture are calculated in a manner similar to those for beta transitions.

The best method to determine the maximum beta-ray energy experimentally is to compute a Fermi-Kurie plot.[15] From Equation 2 one can derive the following equation for an allowed beta spectrum

$$N(\eta) = (\text{const})\ F(Z,\eta)\ \eta^2\ (\varepsilon_o - \varepsilon)^2\ , \qquad (3)$$

where $N(\eta)$ represents the number of beta rays detected with momentum η. By plotting $[N(\eta)/\eta^2 F(Z,\eta)]^{1/2}$ as a function of ε a straight line is obtained with an intercept at $\varepsilon = \varepsilon_o$.

If the beta distribution contains beta rays of different end points, the plot of the high-energy component will be straight until the end point of the low-energy beta ray is reached. The second component can be

subtracted by extrapolating the straight line from the high energy component back to the ordinate. At nearly any energy, then, the number of counts from the high-energy beta ray can be determined from the square of the corresponding ordinate value. These counts, in turn, can be subtracted from the total number of counts at the value of ϵ in question to obtain the counts for the low-energy, beta-ray component. A separate plot for the low-energy spectrum will give the end point for the beta ray also. This same procedure may be followed for any additional components.

3. Nuclear-Reaction Spectroscopy

Another aid in the analysis of nuclear decay schemes is the information derived from inelastic nuclear reaction studies. When a nucleus is bombarded with a particle of measured energy, the particle may excite the nucleus and may be re-emitted with an energy less than the bombarding energy. The difference between the energies of particles emitted from the ground state and from an excited state corresponds to the excitation energy of that level. When it interacts with the nucleus the particle will give up some of its angular momentum and the differential cross section as a function of angle will depend upon the momentum transferred. Thus by detecting the energy of the emitted particles at various angles, one can measure energy levels and often can deduce the spins. Experimentally only levels corresponding to small amounts of angular momentum transferred will be strongly excited. Sometimes peaks are too weak to determine accurately the change in cross section with angle. Such nuclear reaction spectroscopy studies often complement data obtained

in studies of nuclear decay schemes, since states may be excited in nuclear reactions which are not seen in radioactive decay.

C. SPECTROSCOPY OF THE MASS-89 REGION

All of the effective-interaction calculations in the mass-90 region[9,10,11] have involved nuclei heavier than ^{90}Zr and only the $d_{5/2}$, $s_{1/2}$ and $g_{7/2}$ neutron orbitals. This dissertation will discuss the neutron deficient nuclei lighter than mass-90 which would involve $g_{9/2}$ neutron holes. Such results shed light on particle-hole and hole-hole interactions. The levels of ^{89}Y, ^{89}Zr, and ^{89}Nb exhibit these types of interactions.

Properties of states in the mass-89 region are determined largely through filling the $2p_{1/2}$ and $1g_{9/2}$ levels with protons and by neutron holes in the $g_{9/2}$ level of the $^{88}_{38}Sr_{50}$ core. This dissertation concerns a study of the levels in ^{89}Y, ^{89}Zr, and ^{89}Nb populated, respectively, by the decays of ^{89}Zr, ^{89}Nb, and ^{89}Mo.

In the decay chain of neutron deficient isotopes of mass-89, all isotopes have isomers because of the large spin change between the two low-lying $g_{9/2}$ and $p_{1/2}$ states. The decay of ^{89}Zr and $^{89}Zr^{m}$ will be discussed first, because it is at the"end" of the decay chain. The information obtained from the decay of ^{89}Zr and $^{89}Zr^{m}$ is needed to study the decay of the parent isomers, ^{89}Nb and $^{89}Nb^{m}$, which in turn, is needed to study the decay of ^{89}Mo and $^{89}Mo^{m}$.

As one moves away from the "region of stability" along the decay chain, one expects the Q value (energy difference between the ground

states of the parent and daughter isotopes) to be greater. It follows that the half-life will be shorter for the parent and that the emitted beta and gamma rays will be more energetic.

The levels of $^{89}_{39}Y_{50}$ are influenced by the interaction of a $p_{1/2}$ proton with the closed shell of $^{88}_{38}Sr_{50}$. From Figure 1 it can be predicted that the first excited state may be $9/2^+$ (the superscript denotes parity), if the proton is raised to the $g_{9/2}$ level. Another predicted excited state is $3/2^-$, which corresponds to decoupling a $p_{3/2}$ proton pair and raising one proton to the $p_{1/2}$ orbital, where it couples to zero with the $p_{1/2}$ proton. The remaining $3/2^-$ hole determines the spin and parity of the state. In a similar manner an $f_{5/2}$ proton coupled to the $p_{1/2}$ proton creates a $5/2^-$ level. Other levels may correspond to the lone proton rising to the $1g_{7/2}$ or the $2d_{5/2}$ proton states.

The levels of $^{89}_{40}Zr_{49}$ involve the interactions between protons in the $g_{9/2}$ and $p_{1/2}$ levels with neutron holes. As with ^{89}Y, one can predict the first excited states as $1/2^-$, $3/2^-$, and $5/2^-$, corresponding to neutron holes in the $2p_{1/2}$, $2p_{3/2}$, and $1f_{5/2}$ levels, respectively. In a similar manner we would look for these spins in levels of $^{89}_{41}Nb_{48}$ populated by the decay of $^{89}_{42}Mo_{47}$.

This dissertation will discuss attempts to verify these states, and, in addition, will present evidence for many more states arising from other interactions.

CHAPTER II

EXPERIMENTAL PROCEDURES

A. INSTRUMENTATION

1. Detectors

Studies of the decay properties of radioactive nuclides require instruments for measuring energy spectra of the emitted radiations. Detectors for such applications must not only announce the arrival of radiation, but also must translate such information into electronic pulses whose amplitude is proportional to the energy of the incoming radiation. These pulses, in turn, must be reshaped and amplified before being sorted in a multichannel pulse-height analyzer.

Three different detectors were used for this study. Anthracene and thallium-activated sodium iodide (NaI) crystals are of the scintillation type, while lithium-drifted germanium [Ge(Li)] detectors are of a solid-state, charge-collection type. The anthracene crystal was used as a beta-ray detector, while the NaI and Ge(Li) detectors were used for gamma-ray analysis.

The incident beta rays excite anthracene molecules along their paths through the crystal. As the molecules de-excite, light photons are emitted which are, in turn, detected by a photomultiplier tube. The energy which the beta ray deposits in the crystal determines how many light photons will be emitted and consequently how large will be the amplitude of the photomultiplier pulse.

Sodium iodide crystals, activated with thallium iodide, emit light quanta when excited by the secondary electrons from gamma-ray interactions in the scintillator. The secondary electrons are produced in several ways. If the incoming gamma-ray energy is low, then an electron may be produced near the surface by the photoelectric effect. A more frequent event above about 100 keV is Compton scattering. In this process a gamma ray interacts with an electron in such a way that the electron and a scattered gamma-ray photon, degraded in energy, share the initially available energy. The degraded photon may escape from the crystal, or may undergo further Compton scattering until the photon energy is so low that photoelectric absorption puts an end to this multiple process. At higher energies, considerably above the energetic threshold of 1.022 MeV, pair production is the dominant interaction of gamma rays with the NaI detector; in this latter process, the high-energy gamma ray disappears and a positron-electron pair is created. The kinetic energy of the pair is transferred to the crystal, but one or both of the 0.511-MeV photons from annihilation of the positron may escape.

If all of the gamma-ray energy is converted to electron kinetic energy, then the scintillation detector produces a number of light photons proportional to the full gamma-ray energy. If annihilation or Compton-scattered gamma rays escape from the crystal, then the number of light photons emitted by the scintillator will be characteristic of an energy transfer smaller than the full gamma-ray energy. The excited state in the NaI crystal which emits the light has a long half-life (250 nsec); however, the quantum yield of this process is high and the emitted light

falls at a wavelength compatible with the commercial photomultiplier tubes used to convert light photon bursts to electronic pulses.

The Ge(Li) detector is a solid state device in which lithium ions have diffused into a crystal of *p*-type germanium (germanium doped with electron acceptors such as boron or gallium) under the influence of a reverse bias voltage (a positive voltage applied on the side treated with lithium and negative voltage applied on the *p*-type germanium side).[16,17] The lithium diffuses deeply into the *p*-type germanium toward the negative potential. The current carried by the lithium ions and electrons will drop to zero when the acceptor concentration has been compensated by the lithium donor concentration. This provides a large region of high resistivity. An incoming gamma ray ionizes the germanium atoms and lifts the ionized electrons into the conduction band. The electrons then travel toward the positive electrode, and the positive charges (electron holes) then travel to the negative electrode creating a weak electronic pulse. As with NaI detectors the greater the energy transferred, the greater will be the amplitude of the output pulse. The band gap in germanium is only 0.66 eV. To reduce electrical noise from thermally excited electrons which cross this gap, the germanium detectors were kept at liquid nitrogen temperature. This also kept the lithium ions from diffusing out of the compensated region.

Many of the peaks in the high-energy portions of spectra are single- and double-escape peaks. A gamma ray above 1.022 MeV may create a positron-electron pair when it stops in matter. The positron from this "pair production" then annihilates with a negative electron and the

rest-mass energy of the two particles appears as two 511-keV photons emitted in opposite directions. If the 511-keV gamma rays escape from the detector, the detector will produce a pulse which corresponds to the full energy of the incoming gamma ray less 1022 keV. Consequently, the spectrum will show a "double escape" peak, 1022 keV lower in energy than the full-energy peak. If only one 511-keV gamma ray escapes, a "single escape" peak will appear 511 keV below the full-energy peak. As the energy of the gamma ray increases, the cross section for pair production increases. Higher-energy gamma rays have larger double-escape peaks.

Resolution is defined as the full width at half maximum (FWHM) of the full-energy peak. The resolution of the anthracene crystal for internal conversion electrons was measured as 17 per cent (106 keV at 624 keV). On the other hand, the average resolution of the NaI detector for gamma rays was 7.5 per cent (50 keV at 662 keV). The Ge(Li) detectors have much better resolution than NaI detectors but have a much smaller sensitive volume and consequently are much less efficient. In all of the studies reported here, the disintegration rate was high enough to use Ge(Li) detectors with volumes of 6 cm^3, 20 cm^3, and 35 cm^3. The average resolution of the three detectors was approximately 0.22 per cent (3 keV at 1332 keV). Peak widths increase with energy in a complicated way for all three types of detectors.

2. Amplifying Systems

For the anthracene and NaI crystals amplification was provided by a ORNL Model A-8 amplifier and preamplifier. A preamplifier was used near the detector to cut signal losses. A decrease in signal-to-noise

ratio would be apparent if there were a long cable connecting the detector with the amplifier. The preamplifier can be used at an electronic gain of 1, 3 or 10. Some of the attributes of the A-8 amplifier are its ability to recover rapidly from very large overload pulses (from detection of mesons and high-energy gamma rays), its tolerance of high counting rates (100,000 counts/sec), and its short output pulse width (1.1 μsec). Since it is a vacuum-tube amplifier it has the disadvantage of high heat dissipation and large size. The output pulse of the A-8 amplifier can be as high as 100 volts.

Noise signals tend to broaden spectral lines and degrade the resolution. For scintillation counting the major source of noise is due to the release of electrons by thermal agitation at the photoelectrode of the photomultiplier tube. Another source of noise arises from thermal motion of electrons in the input grid resistor of the amplifier. Scintillation detectors generally produce large signals with relatively poor resolution, so these sources of noise do little to worsen the resolution.

However, the noise problem becomes serious for semiconductor radiation detectors, because the detector output pulse is of low amplitude and the detector is capable of high resolution. Since the signal amplitudes are so low the amplifier does not need to have a high overload performance. For Ge(Li) detectors the following low noise TENNELEC equipment was used: preamplifier (TC-135), amplifier (TC-200), and biased amplifier (TC-250).

The secondary gamma-ray reactions excite electrons into the

germanium conduction band. The electrons are quickly attracted to the positive terminal, but the electron holes have only one third the mobility of electrons. Thus the negative output pulse will rise sharply and decay slowly. The rise time for a 20 cm^3 detector is about 50 nsec.

The TC-135 is a charge-sensitive preamplifier with a very high input impedance and a low-noise field-effect transistor (FET) at the input stage. The preamplifier provides considerable gain before the pulses are sent over a cable to the TC-200 amplifier; this technique reduces noise contributions by the cable. The output pulse of the TC-135 has a rise time (the time required for the pulse to gain 63 per cent of its maximum amplitude) of about 200 nsec and a decay time of 2 msec.

Because of such a long "tail" on the preamplifier output pulse, other pulses are generally superimposed on each other. The amplifier must not only amplify the pulse but reshape it to prevent overlap. In addition, the reshaping circuits filter the noise, enhancing the signal-to-noise ratio.

The TC-200 amplifier has a CR differentiation circuit and a RC integration circuit. The CR differentiation circuit affects the decay of the output pulse and attenuates the low frequency noise. The RC integration circuit determines the rise time of the output pulse and filters high frequency noise as shown in Figure 3. A combination of the circuits will form a pulse with a fast rise time and a relatively short decay time constant relative to the preamplifier pulse. On the TC-200 the capacitors and resistors can be changed to provide a wide

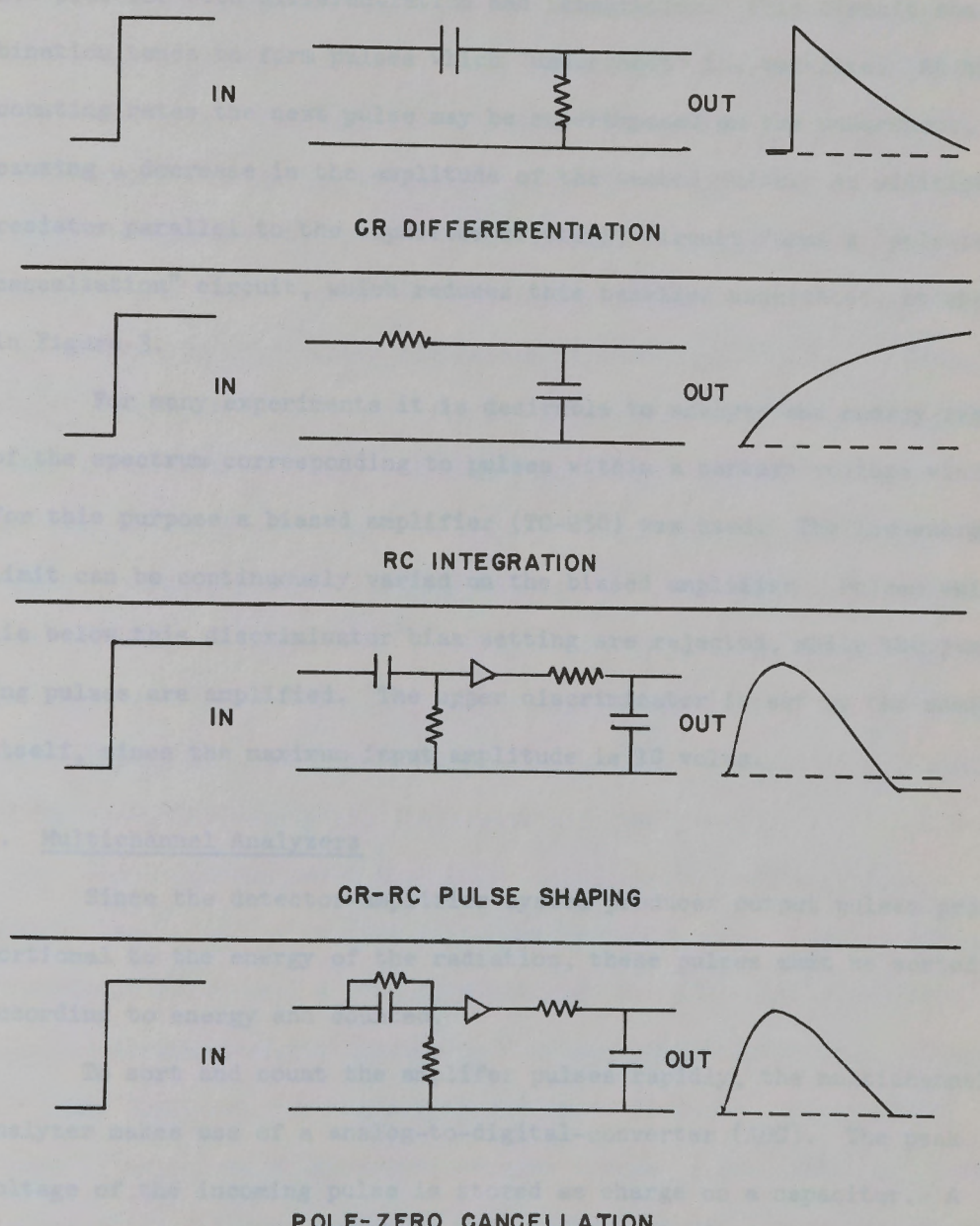


Figure 3. Pulse shaping circuits used in the TC-200 amplifier.

range of time constants. Time constants used for the experiments were 1.6 μsec for both differentiation and integration. This circuit combination tends to form pulses which "undershoot" the baseline. At high counting rates the next pulse may be superimposed on the undershoot, causing a decrease in the amplitude of the second pulse. An additional resistor parallel to the capacitor of the RC circuit forms a "pole-zero cancellation" circuit, which reduces this baseline undershoot, as shown in Figure 3.

For many experiments it is desirable to analyze one energy region of the spectrum corresponding to pulses within a certain voltage window. For this purpose a biased amplifier (TC-250) was used. The low-energy limit can be continuously varied on the biased amplifier. Pulses which lie below this discriminator bias setting are rejected, while the remaining pulses are amplified. The upper discriminator is set by the analyzer itself, since the maximum input amplitude is 10 volts.

3. Multichannel Analyzers

Since the detector-amplifier system produces output pulses proportional to the energy of the radiation, these pulses must be sorted according to energy and counted.

To sort and count the amplifer pulses rapidly, the multichannel analyzer makes use of a analog-to-digital-converter (ADC). The peak voltage of the incoming pulse is stored as charge on a capacitor. A logic circuit initiates the linear discharge of this storage capacitor and simultaneously turns on a "clock" oscillator. When the storage capacitor voltage has dropped to an arbitrary reference voltage level,

the oscillator is stopped, and a count is stored in a location of the ferrite-core memory corresponding to the number of pulses produced during the discharge of the storage capacitor. For example, a Nuclear Data 4096-channel analyzer has a 16 MHz[18] oscillator and requires 66 nsec/channel to digitize an analog signal. The information is stored in a ferrite-core memory. When a pulse arrives at a particular memory location, the number stored in that location is read out into a scaler, one is added to it, and the new number is stored in the same location. It requires approximately 25 μsec to store a count. On the average it takes 150 μsec to digitize and store each count of a typical spectrum recorded at the Nuclear Data Analyzer. During this time the analyzer cannot analyze any more incoming pulses. At a counting rate of 10,000 counts/sec the analyzer will be counting almost 100 per cent of the time, but will be able to count only 70 per cent of the pulses, while for a counting rate of 1000 counts/sec the ADC will count about 15 per cent of the time, but nearly all the counts will be recorded.

The Victoreen Model MP-204 RT 20,000 channel multiparameter analyzer has a set of two ADC units denoted as X and Y. The memory can be subdivided into 100 × 200, 50 × 400 and 20 × 1000 matrices. For coincidence measurements the memory was used as a 50 × 400 matrix whereby the Y ADC digitized the incoming pulse amplitudes over a span of 50 channels, while the X ADC digitized over a span of 400 channels. Each time an event occurred in both X and Y detectors and a coincidence gate signal arrived simultaneously, the X and Y addresses generated by the two ADC units registered an event in the 50 × 400 memory matrix. For

singles measurements the 20 × 1000 mode was used, whereby 20 successive 1000-channel spectra could be recorded in the memory.

Two other multichannel analyzers were used for singles experiments: a 1600-channel Victoreen SCIPP and a 4096-channel Nuclear Data. To prevent amplifier gain shifts a stabilizer was used with the 4096-channel analyzer to readjust the gain so that a pulser peak, counted simultaneously with the spectrum, was always recorded in the same channel.

The ADC of a multichannel analyzer is never exactly linear and a calibration must be made to correct for this non-linearity. This correction was made by using a precision pulse generator. Pulses with a precise amplitude interval were fed into the preamplifier so that the non-linearity of the entire amplification and analyzer system could be checked. With the keV/channel calibration slope accurately determined by the pulser, the deviation of each channel was plotted versus the channel number. The graph then gave the correction that must be made to the experimental position of each gamma-ray peak in order to obtain a linear relationship between energy and peak position.

Data from the 20,000-channel analyzer were read onto magnetic tape. Data from the 1600-channel and 4096-channel analyzers were punched on paper tape with a high-speed punch in binary-coded decimal code. The data were then transferred to magnetic tape by a CDC-160-A computer.

4. Instruments for Timing

Gamma rays are said to be in coincidence if they are emitted from the same nucleus in a cascade type of decay within the resolving time of the electronic system. To make coincidence measurements several detectors,

their respective amplifiers, and fast timing instrumentation were used. The fast timing instruments employed were manufactured by ORTEC. These were time pickoff units, time pickoff control, timing single-channel analyzers, gate and delay generators, delay amplifiers, linear gates, and fast-coincidence circuits.

The time pickoff unit "senses" charge collection by the detector and generates a logic pulse of fast rise time which is almost independent of the energy of the detected gamma ray, and correlated in time with the leading edge of the detector pulse. The output pulse is a square-shaped logic pulse necessary for the input of a coincidence circuit. The time pickoff control contains the power supply for the time pickoff unit and also has a discriminator to control the detector pulse amplitude needed to trigger an output pulse. Normally the discriminator trigger level is set just above the noise level.

When in the differential mode the timing single-channel analyzer triggers on pulses of a given amplitude E within a certain pulse-height interval ΔE. When these requirements are met it generates a logic signal. The logic signal may be delayed by an interval time-delay unit from 0 - 1 μsec. Both E and ΔE may be varied as required by the spectrum under study. When in the integral mode, all pulses greater than amplitude E are counted. In either the integral or differential mode, the timing single-channel analyzer produces an output signal which coincides with the time the positive part of the doubly-differentiated amplifier signal crosses the baseline to the negative part.

The gate and delay generator produces logic pulses of selected

polarity, width and amplitude, when triggered by a positive logic pulse. Also, the pulse may be delayed for coincidence timing. For gamma-gamma coincidence measurements, the gate and delay generator was used to invert the positive output pulse of the coincidence circuit and increase the pulse width suitably for opening the coincidence gate on the 20,000 channel multiparameter analyzer.

Delay amplifiers simply delay a pulse without reshaping it. Various amounts of delay from 0.25 - 4.75 μsec can be added to the circuit. These were used to delay amplified Ge(Li) and NaI detector signals so that they would not reach the analyzer before the coincidence pulses arrived. A linear gate produces an output pulse whose height is proportional to that of the input pulse when an "enable" pulse appears.

A fast coincidence circuit produces a logic pulse whenever input pulses arrive within the resolving time of the circuit. A double coincidence circuit requires that two pulses arrive at two input terminals at nearly the same time, while a triple coincidence circuit requires three simultaneous input pulses. The resolving time of the fast coincidence circuits used in this study could be varied from 10 nsec to 110 nsec.

5. Gamma-Gamma Coincidence Counting System

A gamma-gamma coincidence spectrometer was assembled from the detector, amplifier, and logic components described above. A functional block diagram of the system is shown in Figure 4. ORTEC instrument numbers are shown in the blocks representing timing instruments.

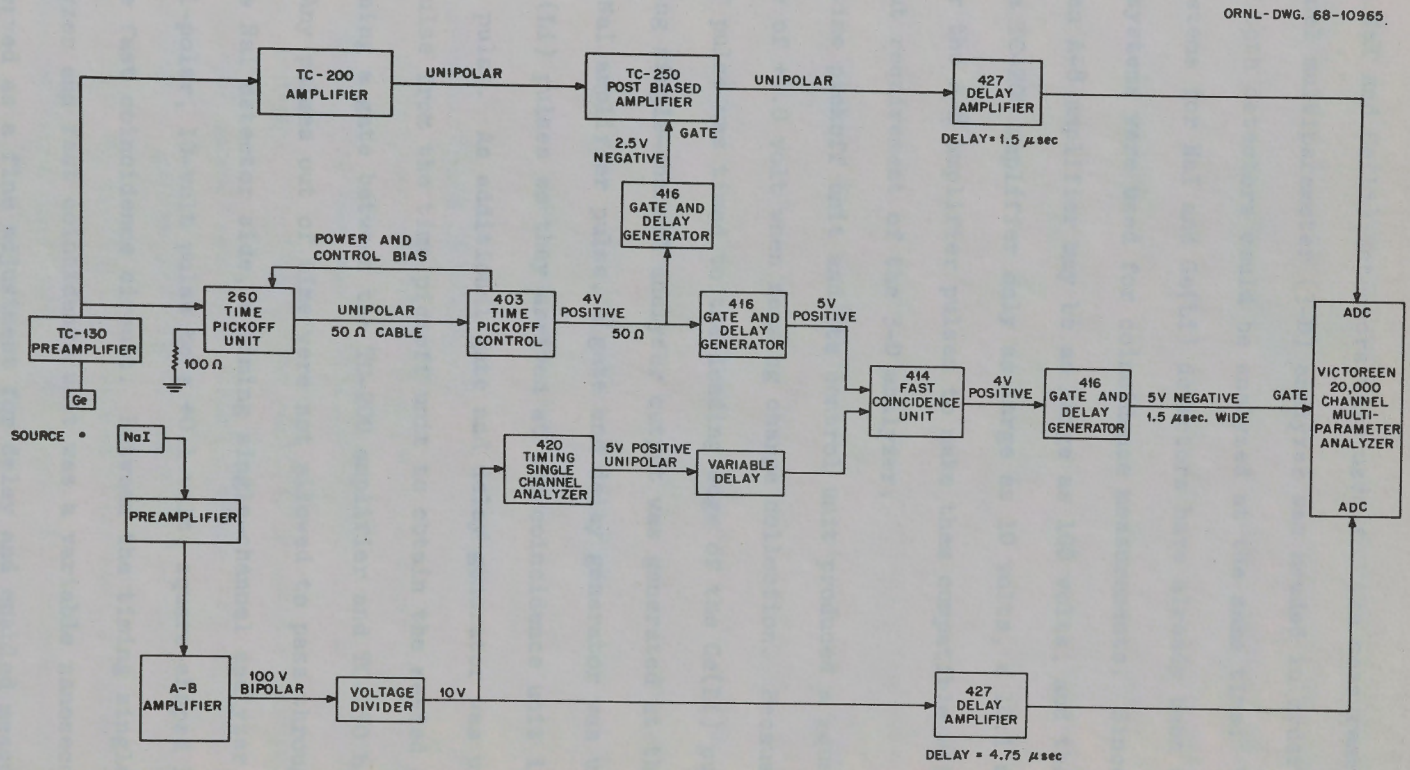


Figure 4. Block diagram of electronic system used in the Ge(Li)-NaI coincidence experiments.

Both NaI and Ge(Li) detectors were used for the measurements. The 20,000-channel multiparameter (3-D) analyzer was needed in order that pulses from both detectors could be analyzed at the same time. The amplification systems for NaI and Ge(Li) detectors have already been explained. These same systems were used for coincidence measurements. Since the NaI pulse from an A-8 amplifier may be as large as 100 volts, and the Ge(Li) pulse from a TC-200 amplifier only as large as 10 volts, a 10:1 attenuator was used for the A-8 amplifier pulses to make them compatible with the 10-volt input requirement of the 3-D analyzer.

The time pickoff unit and its control unit produced a square-shaped pulse of +4.0 volt when sensing charge collection. Because the time pickoff pulse was timed to the leading edge of the Ge(Li) pulse and the timing single-channel analyzer output was generated at the cross-over of the NaI amplifier pulse, a gate and delay generator was used to delay the Ge(Li) pulses so they arrived at the coincidence unit in time with the NaI pulse. An additional gate and delay generator was used to invert the pulse from the time pickoff unit to obtain the needed -0.5 volt for opening a gate between the TC-200 amplifier and TC-250 biased amplifier. Any pulses out of time were not allowed to pass through the gate. On the NaI detector side, a timing single-channel analyzer converted the bi-polar, 10-volt pulse to a +0.1-volt, square-shaped logic pulse for the fast coincidence circuit. Between the timing single-channel analyzer and fast coincidence unit was a variable nanosecond delay box. This served as a fine adjustment for delay and enabled measurement of the resolving time curve of the system.

When the logic pulses arrived within the resolving time of the coincidence unit, one positive logic pulse was produced. The pulse needed to open the coincidence gate of the 3-D analyzer must be -5.0 volts and 1.5 μsec wide. The coincidence output pulse was modified to meet these specifications by use of a gate and delay generator. The gate must be opened 200 nsec before the X and Y pulses arrive. Delay amplifiers delayed both X and Y pulses so they did not arrive before the coincidence gate signal.

The 20,000-channel multiparameter analyzer was programmed so that it would count pulses from only one detector (singles) for an indicated period of time, then count pulses from the other detector for the same period of time, and finally count coincidence events for a longer period of time. Then the analyzer would recycle and follow the same procedure as long as desired. These singles measurements were needed to correct for random coincidence events as described later.

6. Positron Scintillation Spectrometer

Positrons were detected with an anthracene scintillation detector. As a positron passes through the scintillator, ionization occurs and the positron loses energy. Eventually the positron stops and annihilates, forming two 511-keV gamma rays which usually escape the crystal. Gamma rays may also produce pulses by interacting with the crystal through Compton scattering. To distinguish between these events the beta-gamma coincidence system shown in Figure 5 was used. Anthracene detector pulses were accepted by the analyzer only when two 511-keV gamma rays were seen; a triple coincidence between the two NaI detectors and the

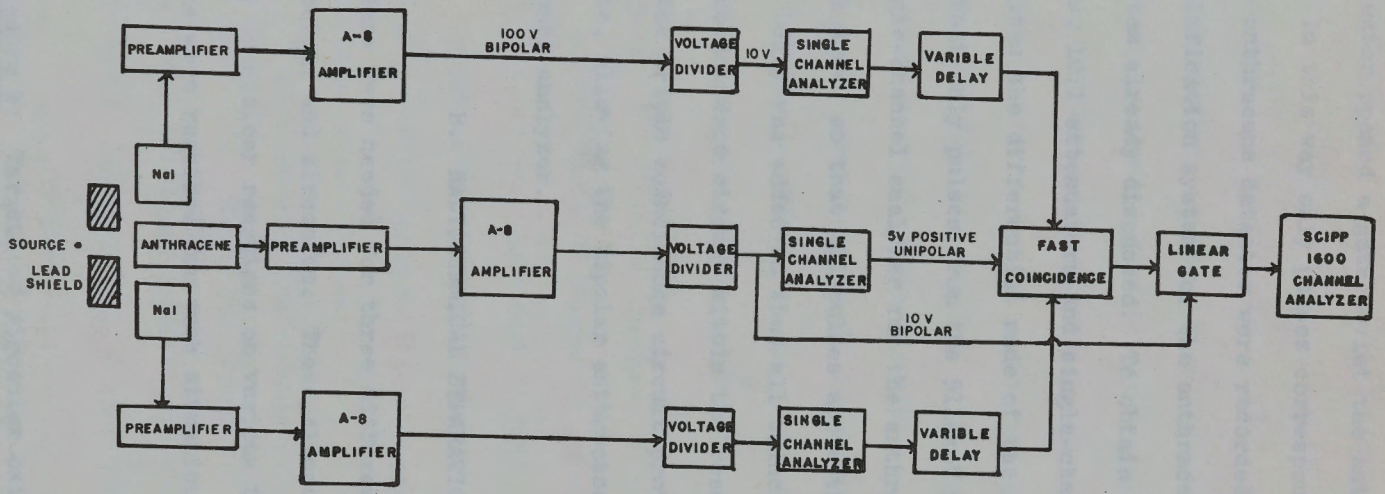


Figure 5. Block diagram of electronic system used to measure positrons.

anthracene detector opened a gate to let the anthracene pulse pass to the analyzer. In this way only pulses corresponding to positrons which stopped in the anthracene detector were recorded.

The amplification system for the anthracene detector was the same as the NaI system already discussed. To obtain logic pulses from all three detectors, 10:1 attenuators and single-channel analyzers were used. For the NaI pulses the differential mode of the single-channel analyzers were used, so that only pulses from the 511-keV peaks gave a logic signal. The timing single-channel analyzer for the anthracene channel operated in the integral mode, so that all pulses above the noise level gave a logic signal. Delay was added so that all coincidence pulses arrived at the triple coincidence circuit within the resolving time of 50 nsec. The output of the triple coincidence circuit provides an enabling pulse to a linear gate, allowing the bipolar anthracene pulse to pass to the SCIPP 1600-channel analyzer.

B. RADIOCHEMICAL SEPARATIONS

Separations were needed for three different elements, namely, molybdenum, niobium, and zirconium. These elements were made in several different types of nuclear reactions on various targets. Specific chemical separations were required for each situation.

1. Molybdenum

a. Procedure 1: Targets of zirconium oxide enriched in ^{90}Zr were bombarded with He ions to make molybdenum, niobium, and zirconium

activities. The ability of zirconium and niobium to carry on iron(III) hydroxide was used as the basis of this separation. The zirconium oxide target was dissolved in a teflon dish containing 1 ml of hot 27 M hydrofluoric acid. Molybdenum carrier (20 mg), iron carrier (10 mg), and niobium carrier (10 mg) were added to this solution. The solution was made basic by adding 8 ml of 7 M ammonium hydroxide. The iron(III) hydroxide was filtered on a fritted glass funnel. To the filtrate was added 10 ml of 4 M nitric acid and 3 ml of 2 per cent α-benzoin oxime. The molybdenum precipitate was washed first with 1 M nitric acid and then with water, and finally counted. Chemistry was completed in less than 4 min, but it required 5 min to transfer the target from the cyclotron building to the chemistry laboratory.

b. Procedure 2: Chloride complexes of molybdenum(VI) are soluble in ether. This was the basis of separation of molybdenum from niobium and zirconium activities when potassium niobate targets were bombarded with protons. The potassium niobate was dissolved in 5 ml of solution containing 1 ml of potassium bromate (to be certain the molybdenum ions were in their highest oxidation state), 3 ml of molybdenum carrier solution (30 mg) and 1 ml of water. The solution was made acidic with 5 ml of 12 M hydrochloric acid. The white niobium(V) oxide precipitated and was filtered off. The remaining solution was then contacted with 10 ml of diethyl ether, which had been presaturated with 6 M hydrochloric acid. The ether was then "back-extracted" with water and the molybdenum was precipitated with 4 ml of 2 per cent α-benzoin oxime in ethanol. This was filtered and washed with 1 M nitric acid and then with water.

c. Procedure 3: Proton bombardments of molybdenum makes three different elements: technetium, molybdenum, and niobium. Niobium and technetium were separated first; molybdenum was then precipitated and counted. A molybdenum(VI) solution was made by dissolving 100 mg of metallic molybdenum enriched in ^{92}Mo, in 4 M nitric acid. This solution was then irradiated in a 2-ml aluminum cell. Immediately after the bombardment stopped, the solution was forced out of the cell by compressed air and into a solution containing 1 ml of iron(III) carrier (10 mg) and 3 drops of rhenium(VII) carrier (1 mg). The solution was then made basic with a solution containing 2 ml of 7 M ammonium hydroxide and 1 ml of saturated tetraphenyl ammonium chloride. Two precipitates then formed, ferric hydroxide and tetraphenyl arsonium perrhenate, together with the small amount of a technetium which was carried down with the rhenium precipitate. These precipitates then were filtered with a 60-ml Büchner funnel. The filtrate, containing mostly molybdenum, was made acidic with 6 ml of 4 M nitric acid. This solution then flowed into 6 ml of 2 per cent α-benzoin oxime. Niobium "holdback" carrier (20 mg), complexed with oxalic acid, prevented any radioactive niobium which might not have been carried down with the iron from being carried on the molybdenum precipitate. The molybdenum precipitate then was centrifuged, washed first with 1 M nitric acid and then with water, and finally counted.

All steps to centrifuging the molybdenum precipitate were done by use of remote controls and a closed-circuit television monitor outside the experimental room. A large plastic box surrounded the entire

apparatus to prevent possible spread of radioactive contamination. In Figure 6 is shown an over-all view of the apparatus which emphasizes the magnetic quadrupole lens used to focus the ion beam of the cyclotron on the target, shown at the right. Details of the automatic chemistry system are shown in the photograph of Figure 7.

d. Procedure 4: Twenty mg of metallic molybdenum powder, enriched in ^{92}Mo, was placed in a test tube and irradiated. At the end of bombardment a motor rotated the test tube so that the powder was poured into a test tube containing 3 ml of hot 4 M nitric acid as outlined in Figure 8. The funnel was kept hot with heating tape controlled by a variable autotransformer (Variac). The molybdenum dissolved in about twenty seconds. The dissolved molybdenum and nitric acid then flowed into another funnel containing one ml of iron(III) carrier (10 mg) and 3 drops of rhenium(VII) carrier (1 mg). A solution containing 6 ml of 7 M ammonium hydroxide and 2 ml of a saturated solution of tetraphenyl arsonium chloride was then added, which formed ferric hydroxide and tetraphenylarsonium perrhenate. These precipitates were filtered 150-ml Büchner funnel. To be sure all of the technetium was removed, the filtrate was added to a solution containing 5 ml of water and 1 drop of rhenium(VII) carrier. Tetraphenylarsonium chloride was then added, and the precipitate was centrifuged. The supernatant solution containing the molybdenum activity was poured into a beaker containing 4 ml of 4 M nitric acid, 1 ml of niobium(V) carrier (10 mg) in oxalic acid, and 3 ml of 2 per cent α-benzoin oxime. The molybdenum α-benzoin

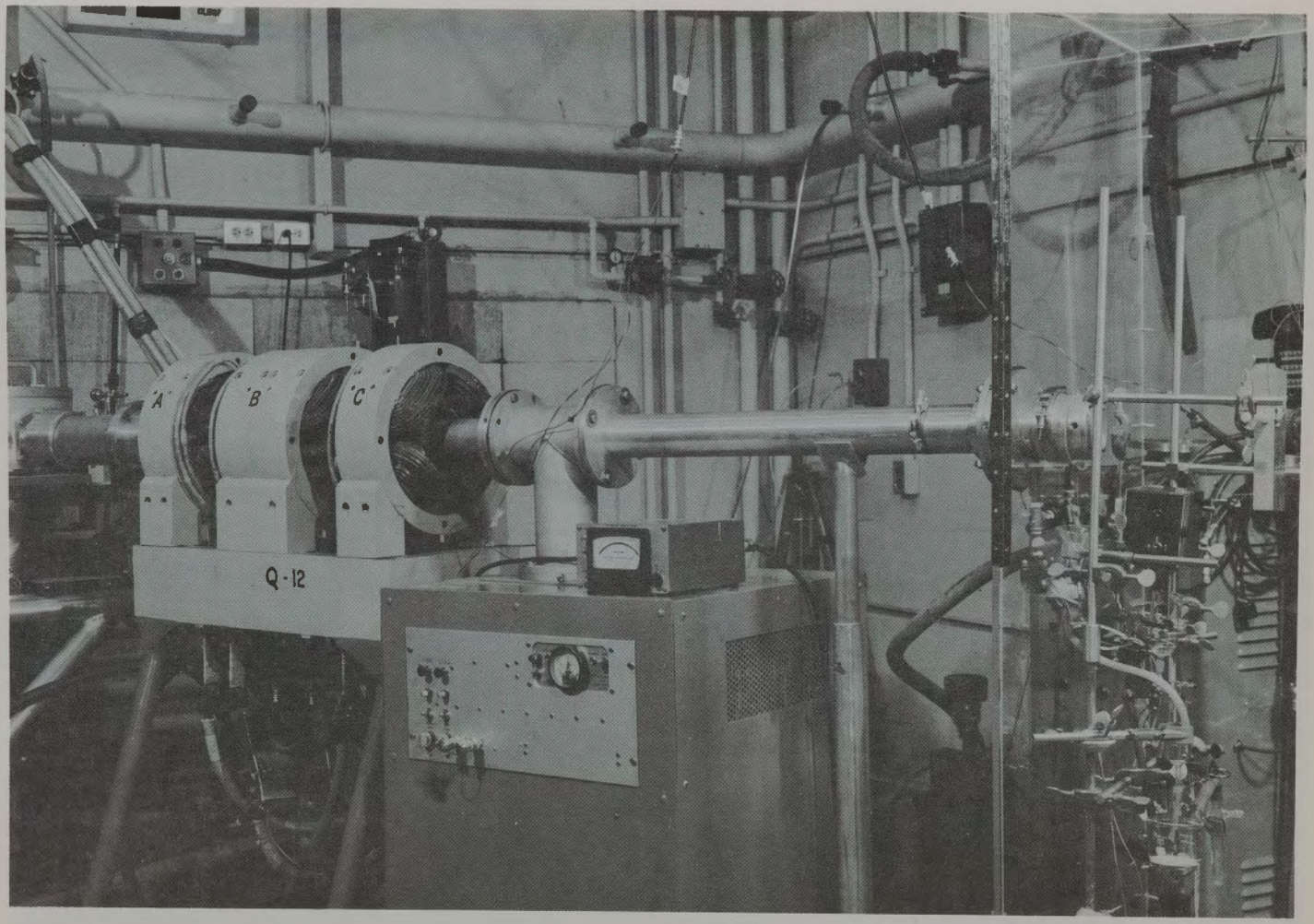


Figure 6. Over-all view of the cyclotron beam pipe showing the molybdenum separation apparatus in relation to the magnetic quadrupole lens.

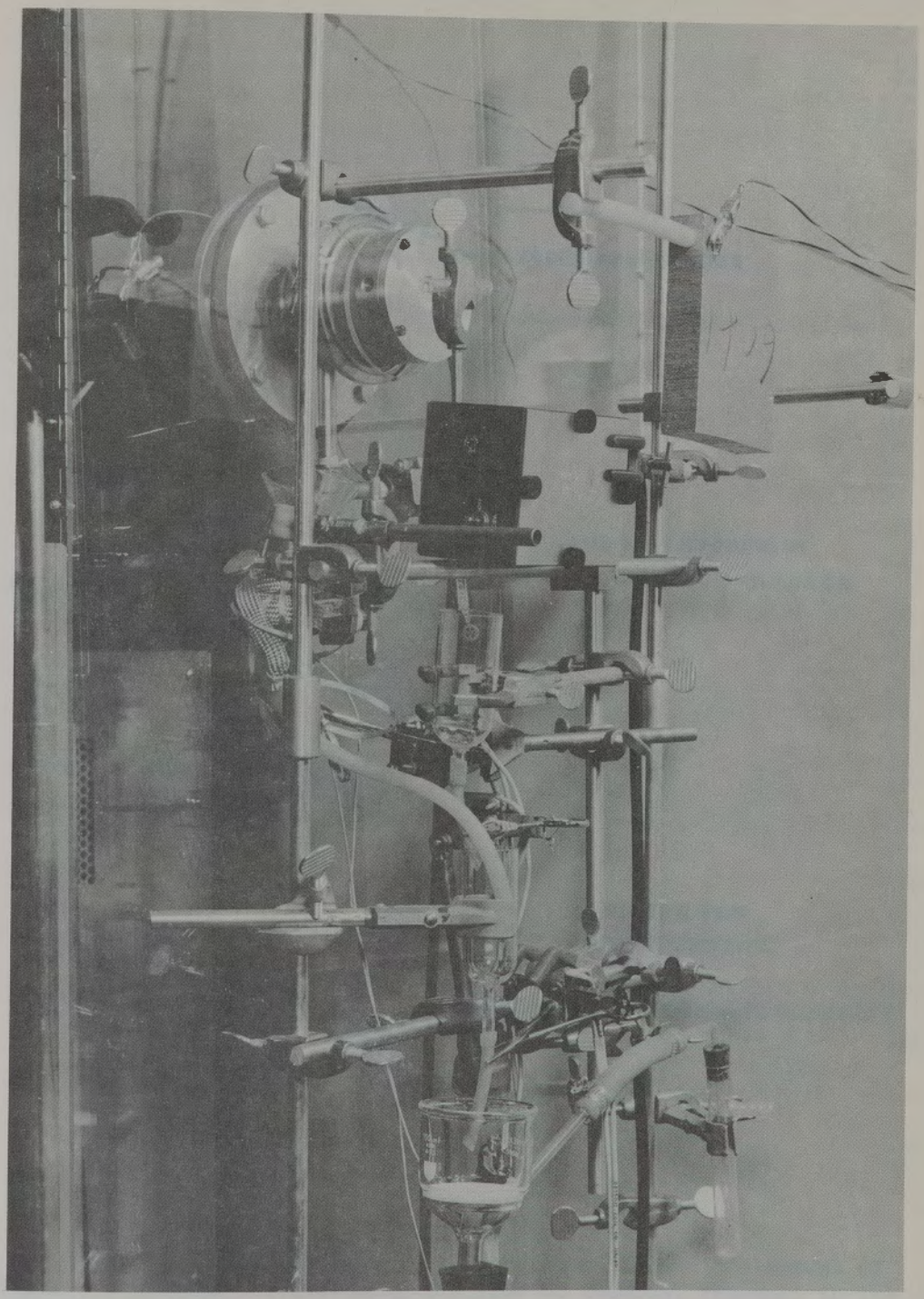


Figure 7. Close-up view of the automatic chemistry system for molybdenum separation.

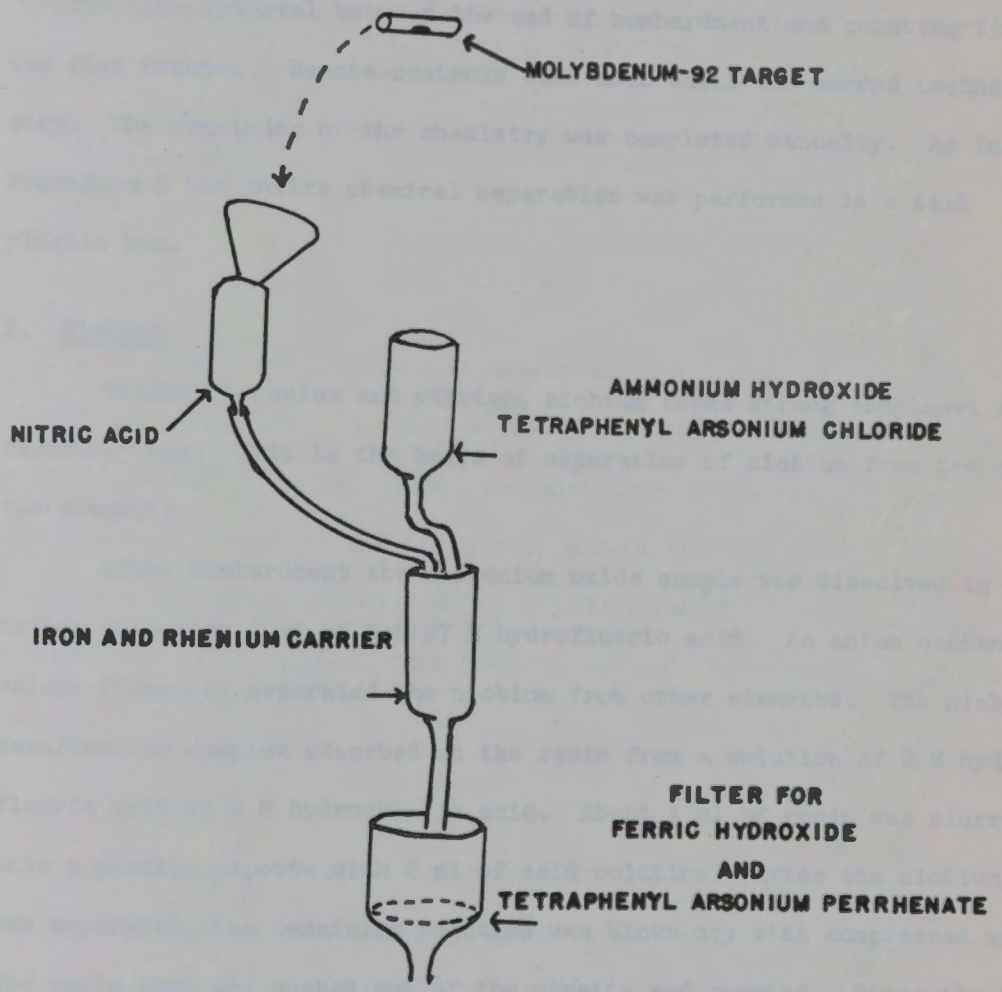


Figure 8. Sketch of chemical equipment in the photograph of Figure 7, showing schematically the flow of chemical reagents in the molybdenum separation.

oxime precipitate then was filtered on a Büchner funnel and washed with ammonium nitrate solution and then with water. The filter paper was folded, placed in a plastic box, and counted.

The time interval between the end of bombardment and counting time was five minutes. Remote controls were used until the second technetium step. The remainder of the chemistry was completed manually. As in Procedure 3 the entire chemical separation was performed in a tall plastic box.

2. Niobium

Unlike zirconium and yttrium, niobium forms strong complexes with fluoride ions. This is the basis of separation of niobium from the other two elements.

After bombardment the zirconium oxide sample was dissolved in a teflon dish with 2 ml of hot 27 M hydrofluoric acid. An anion exchange column (Dowex-1) separated the niobium from other elements. The niobium hexafluoride complex adsorbed on the resin from a solution of 2 M hydrofluoric acid in 9 M hydrochloric acid. About 1 ml of resin was slurried into a plastic pipette with 2 ml of acid solution. After the niobium was separated, the remaining solution was blown dry with compressed air. The resin then was pushed out of the pipette and counted. Since the top of the resin had the greatest specific activity, only the top fraction of the column was counted.

3. Zirconium

For the study of zirconium the same procedure was used as for the

niobium separation, except zirconium(IV) was precipitated from the eluting agent as barium fluorzirconate by adding 1 ml of barium nitrate [10 mg barium(II)]. The precipitate was filtered in a Büchner funnel, washed with water, and counted. Since ^{89}Nb decays to ^{89}Zr, zirconium was continually forming and was washed from the column with more eluting agent. Niobium stayed on the column. The samples were counted about four minutes after elution.

C. DATA ANALYSIS

Most experiments required accumulating many spectra of 1000, 1600, or 4096 channels each. To plot these data quickly and analyze the peaks for area, energy, and half-life, computer programs were needed to process the vast amount of data collected during the experiment. The programs used in this study were TAPE, KORRECT, DAZYMA, FYSREV, FRANTIC, and KURIE. These programs were used on the CDC 1604-A and IBM 360/75 computers.

1. Program TAPE

To conserve the number of magnetic tapes used by an experimenter, program TAPE[19] was used to store the data accumulated by the 20,000 channel multiparameter analyzer. Data were transferred from the magnetic tape used during the experiment, and placed in an assigned position on a high density storage magnetic tape, where the data could later be relisted. As many as 50 sets of 20,000-channel spectra could be stored on the magnetic tape. Once on the magnetic tape program TAPE

then sums or subtracts up to 8 sets of 20,000-channel spectra and any number of planes; then, it lists and generates a plot tape of the desired X or Y planes. Plots were generated by a CALCOMP plotter which used commands stored on the plot tape.

2. Program KORRECT

During any coincidence experiment, random radiation will be detected in one detector at the same time (within the resolving time of the system) that radiation is detected in the second detector. The random rate N_R is related to the rates in the X and Y detectors, N_X and N_Y and the resolving time of the system τ.

$$N_R = 2\tau N_X N_Y \ .$$

Thus, for a given channel in a coincidence spectrum the total number of random events N_{RT} will be proportional to the number of events from the X detector N_{XT} and Y detector N_{YT}:

$$\frac{N_{RT}}{(t_c)c} = 2\tau \frac{N_{XT}}{(t_s)c} \frac{N_{YT}}{(t_s)c} \ ,$$

where t_s is the time when only one detector was counting (the X or Y detector) for a cycle, c is the number of cycles and t_c is the counting time per cycle for counting coincidence events. Therefore

$$N_{RT} = K(N_{XT})(N_{YT})$$

where K is a constant containing the resolving time 2τ, the number of cycles c, the coincidence counting time t_c, and the time t_s when only one detector was counting.

Program KORRECT[19] corrected each value in the 50 × 400 coincidence matrix by calculating the random coincident events and subtracting them from the total value. The corrected planes then could be summed, subtracted, plotted and listed in program TAPE.

3. Program DAZYMA

Program DAZYMA[20] finds the peaks and analyzes them for area. If an energy calibration is used, the program calculates the energy of each peak. Likewise, if spectra are taken as a function of time, program DAZYMA also calculates the half-life of each peak. Details of this program are given in the Appendix.

4. Program FYSREV

Program FYSREV[21] reads data from cards or magnetic tapes containing data from the SCIPP 1600-channel and the Nuclear Data 4096-channel analyzers. It then sums or subtracts as many as 50 gamma-ray spectra and then plots the sum. Provision is made for plotting the spectra as linear or log plots. Most spectra in this study were plotted as four cycle log plots. Recently, program DAZYMA has been combined with program FYSREV so that plots and a data analysis can be obtained in one step.

5. Program FRANTIC

Program FRANTIC[22] processes raw counting data and fits the data by least-squares techniques to equations for multiple exponential growth and decay. It is designed to accommodate up to 400 data points and to

analyze for a maximum of 10 components. It is arranged so that several analyses may be made on a given set of data and several sets of data. Several sets of data may be analyzed consecutively. The program reads the data values, such as starting time, time interval and raw counts, from cards.

6. Program KURIE

Program KURIE[20] was used to calculate values for Fermi-Kurie plots from beta spectra. Program KURIE reads the data from a beta distribution whose values are punched on cards or written on magnetic tape. Since the anthracene detector generates a beta spectrum as a function of energy, program KURIE calculates the Fermi function as a function of energy. The program then computes conversion factors needed to make the data values and Fermi functions a function of momentum, instead of energy, to be compatible with Equation 3, in Chapter I.

Program KURIE can sum any number of spectra and channels together, compute the points for a Fermi-Kurie plot, and generate a plot tape. The corresponding plot is then drawn by the CALCOMP plotter.

CHAPTER III

EXPERIMENTAL RESULTS

A. THE DECAYS OF ZIRCONIUM-89 AND ZIRCONIUM-89m

1. Previous Work

The decays of ^{89}Zr and $^{89}Zr^{m}$ were thoroughly investigated by Van Patter and Shafroth[23] by use of NaI gamma-ray detectors. With the advent of high-resolution Ge(Li) detectors the possibility of observing new peaks was greatly enhanced. The present work concerns studies made on the 78-min ground state of ^{89}Zr and the 4.16-min isomeric first excited state, $^{89}Zr^{m}$. Very recently, Hinrichsen[24] also reported Ge(Li) detector measurements of the 78-min ground state.

2. Experimental Procedure

Sources of ^{89}Zr activity were made by bombarding yttrium oxide with 11-MeV protons from the Oak Ridge Isochronous Cyclotron (ORIC). The low energy was chosen to be below the $^{89}Y(p,pn)^{88}Y$ threshold energy. The activity formed was 4-min $^{89}Zr^{m}$, 78-min ^{89}Zr, and 111-min ^{18}F from the $^{18}O(p,n)^{18}F$ reaction. The source was counted after ^{18}F and $^{89}Zr^{m}$ decayed away. No chemistry was necessary.

The half-life of ^{89}Zr was determined by counting the source in a low-background proportional counter for 31 days. The data were fit to a least squares fitting program FRANTIC.[22] A half-life of 78.0 ± 0.2 hr was obtained. Van Patter and Shafroth[23] obtained a value of 78.43 ± 0.08 hr by following the decay of the 909-KeV gamma peak with a NaI detector, in good agreement with the results obtained from the study.

Gamma rays were detected with 6-, 20-, and 35-cm^3 Ge(Li) detectors. At low counting rates the resolutions of these detectors were 2.9 keV and 2.5 keV full width at half-maximum, respectively, for the 1332-keV gamma ray of ^{60}Co. The spectra were recorded with the 1600-channel, 20,000-channel, and 4096-channel analyzers. Figure 9 shows a ^{89}Zr spectrum taken with a 20-cm^3 Ge(Li) detector on the 1600-channel analyzer. In addition to the annihilation radiation and an intense 909-keV gamma peak, four peaks were seen in the 1.7-MeV region. All peaks decayed with a 78-hr half-life.

Sources for $^{89}Zr^m$ were made by bombarding zirconium oxide, enriched in ^{90}Zr, with 27-MeV protons from ORIC. This procedure made 70-min $^{89}Nb^m$ by the reaction $^{90}Zr(p,2n)^{89}Nb^m$. The $^{89}Nb^m$ decayed to $^{89}Zr^m$, which was isolated as described in Chapter II. In this way, 4.16-min $^{89}Zr^m$ activity was available for several hours.

The decay of $^{89}Zr^m$ was followed using twenty successive 40-sec counts on the 20,000-channel analyzer used in the 20 × 1000-channel mode. Only two gamma rays, at 588 keV and 1507 keV, were seen to decay with a short half-life. To search for gamma rays of low intensity, two sources were counted for 12 min while maintaining a constant counting rate by reducing the source-to-detector distance as the source decayed. By this means a high counting rate was prevented, which would broaden the resolution, yet a high total number of counts necessary to observe a low-intensity peak was obtained. No gamma rays were observed between 100 and 3500 keV, except the two peaks mentioned above and low-intensity events due to ^{89}Nb contamination. By using program FRANTIC[22] a half-life

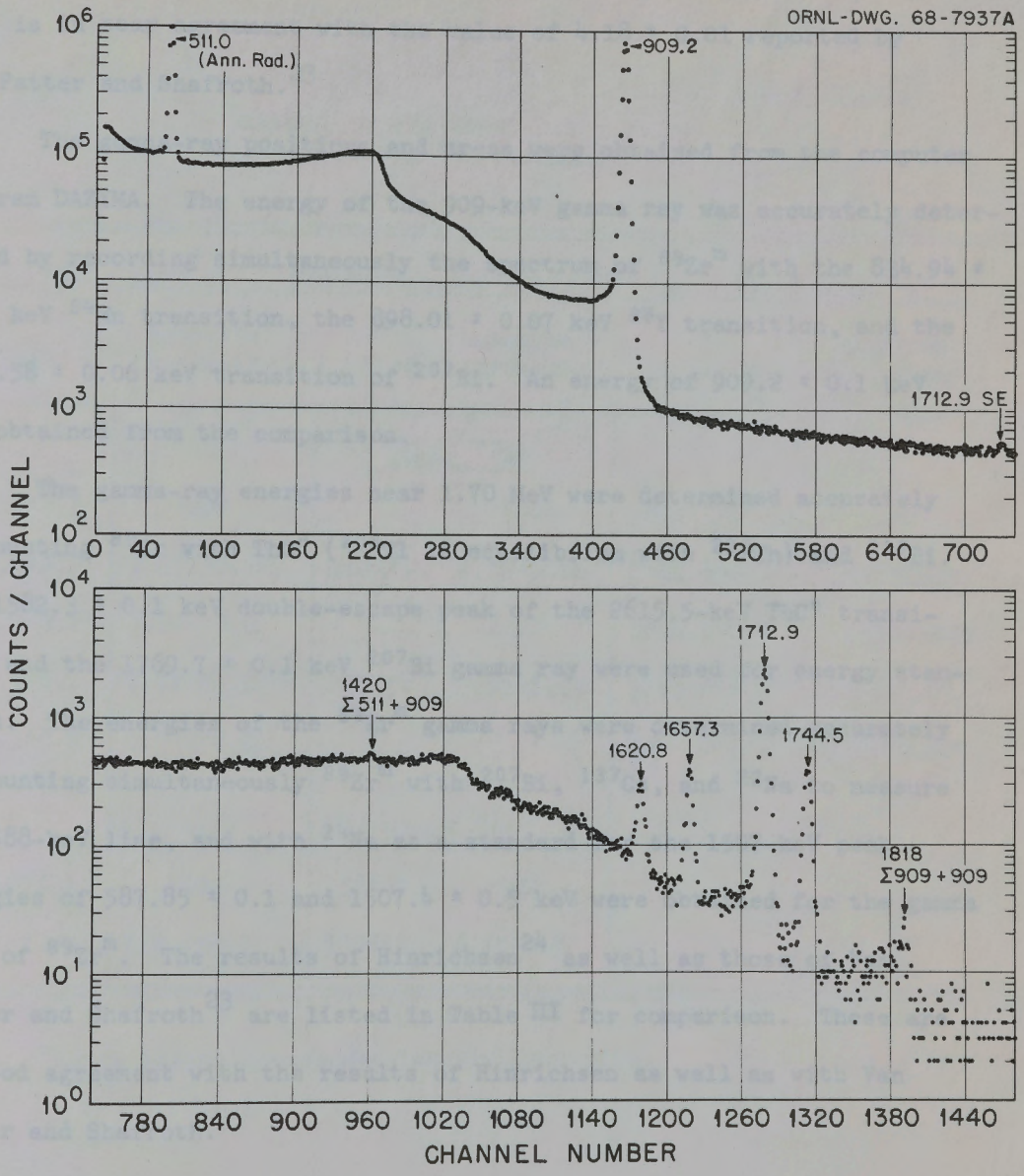


Figure 9. A gamma-ray spectrum of ^{89}Zr taken with a 20 cm^3 Ge(Li) detector.

of 4.16 ± 0.06 min was obtained for the half-life of the 588 keV peak. This is in near agreement with the value of 4.18 ± 0.01 reported by Van Patter and Shafroth.[23]

The gamma-ray positions and areas were obtained from the computer program DAZYMA. The energy of the 909-keV gamma ray was accurately determined by recording simultaneously the spectrum of $^{89}Zr^{m}$ with the 834.94 ± 0.10 keV ^{54}Mn transition, the 898.01 ± 0.07 keV ^{88}Y transition, and the 1063.58 ± 0.06 keV transition of ^{207}Bi. An energy of 909.2 ± 0.1 keV was obtained from the comparison.

The gamma-ray energies near 1.70 MeV were determined accurately by counting ^{89}Zr with ThC" (^{208}Tl in equilibrium with ^{228}Th) and ^{207}Bi. The 1582.3 ± 0.1 keV double-escape peak of the 2615.5-keV ThC" transition and the 1769.7 ± 0.1 keV ^{207}Bi gamma ray were used for energy standards. The energies of the $^{89}Zr^{m}$ gamma rays were determined accurately by counting simultaneously $^{89}Zr^{m}$ with ^{207}Bi, ^{137}Cs, and ^{22}Na to measure the 588-keV line, and with ^{24}Na as a standard for the 1507-keV peak. Energies of 587.85 ± 0.1 and 1507.4 ± 0.5 keV were obtained for the gamma rays of $^{89}Zr^{m}$. The results of Hinrichsen[24] as well as those of Van Patter and Shafroth[23] are listed in Table III for comparison. These are in good agreement with the results of Hinrichsen as well as with Van Patter and Shafroth.

3. Decay Scheme

a. Ground State. The decay scheme proposed for ^{89}Zr and $^{89}Zr^{m}$ is shown in Figure 10. The ground state of ^{89}Y was predicted using the

TABLE III

SUMMARY OF THE GAMMA RAY RESULTS
ON THE ^{89}Zr ISOMERS[a]

This Work		Van Patter and Shafroth[23]		Hinrichsen[24]	
E_γ (keV)	Relative Intensity	E_γ (keV)	Relative Intensity	E_γ (keV)	Relative Intensity
		78-hr ^{89}Zr			
909.2±0.1	100		100	909.1±0.1	100
1620.8±0.2	0.071±0.007	1621±9	0.12±0.01	1620.6±0.7	0.068±0.009
1657.3±0.2	0.10 ±0.01			1656.9±0.7	0.105±0.005
1712.9±0.2	0.77 ± .07	1705±4	0.98±0.03	1713.0±0.6	0.760±0.01
1744.5±0.2	0.13 ±0.01			1744.4±0.7	0.127±0.004
		4-min $^{89}Zr^m$			
587.8±0.1	100	588±2	100		
1507.4±0.5	7.2 ±0.8	1506±5	6.75±0.7		

[a]Error limits represent standard deviation.

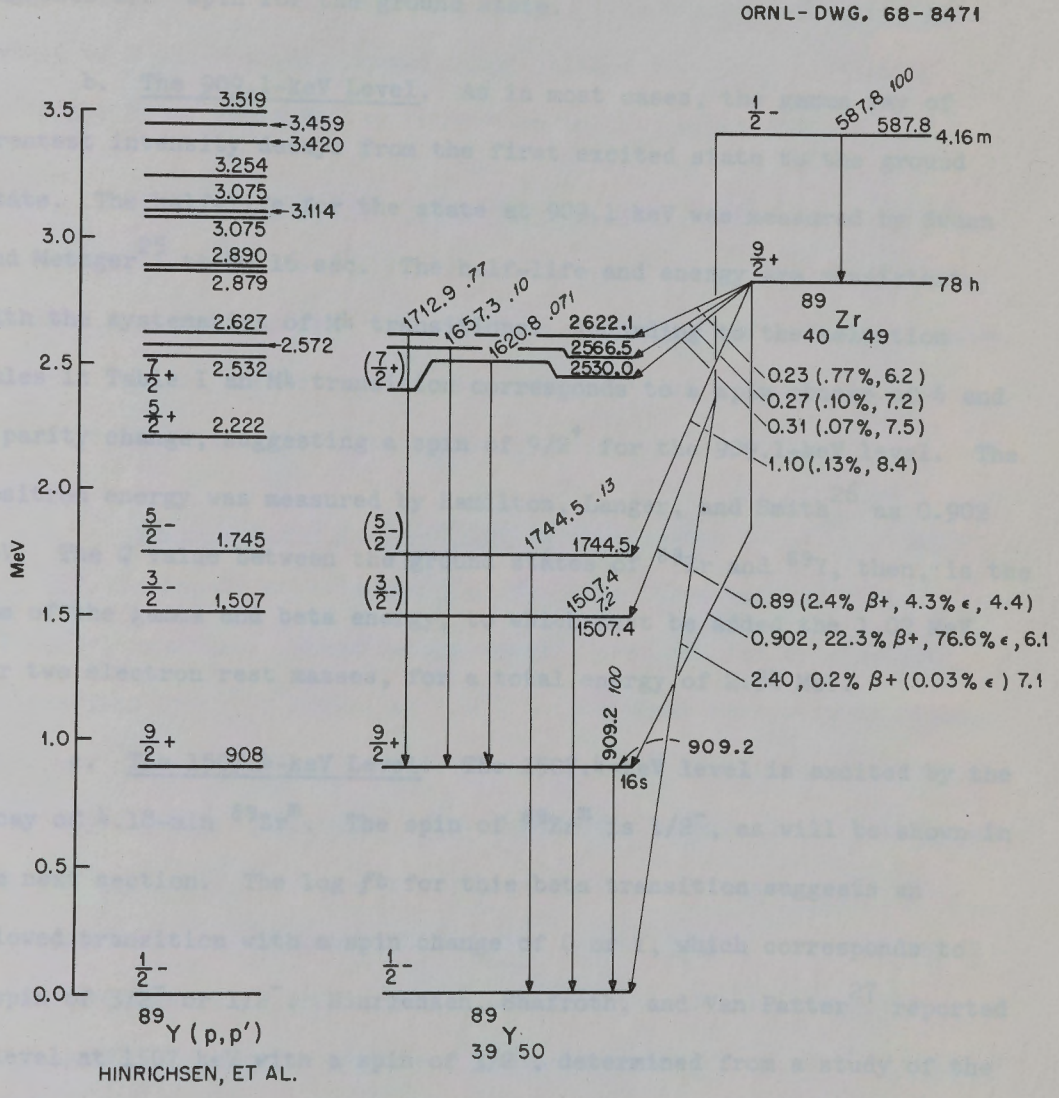


Figure 10. The decay scheme proposed for ^{89}Zr and $^{89}Zr^{m}$. Levels determined by Hinrichsen, Shafroth, and Van Patter[27] from $^{89}Y(p,p')$ reaction work are shown for comparison. Positron and electron capture branches not in parentheses were measured directly by Van Patter and Shafroth.[23]

level order suggested by the shell model of Mayer and Jensen.[1] The ^{89}Y nucleus has 39 protons and 50 neutrons. A proton hole in the $p_{1/2}$ shell suggests $1/2^-$ spin for the ground state.

b. The 909.1-keV Level. As in most cases, the gamma ray of greatest intensity decays from the first excited state to the ground state. The half-life for the state at 909.1 keV was measured by Swann and Metzger[25] to be 16 sec. The half-life and energy are consistent with the systematics of M4 transitions. According to the selection rules in Table I an M4 transition corresponds to a spin change of 4 and a parity change, suggesting a spin of $9/2^+$ for the 909.1-keV level. The positron energy was measured by Hamilton, Langer, and Smith[26] as 0.902 MeV. The *Q* value between the ground states of ^{89}Zr and ^{89}Y, then, is the sum of the gamma and beta energy, to which must be added the 1.02 MeV for two electron rest masses, for a total energy of 2.84 MeV.

c. The 1507.4-keV Level. The 1507.4-keV level is excited by the decay of 4.18-min $^{89}Zr^m$. The spin of $^{89}Zr^m$ is $1/2^-$, as will be shown in the next section. The log *ft* for this beta transition suggests an allowed transition with a spin change of 0 or 1, which corresponds to a spin of $3/2^-$ or $1/2^-$. Hinrichsen, Shafroth, and Van Patter[27] reported a level at 1507 keV with a spin of $3/2^-$, determined from a study of the $^{89}Y(p,p')$ nuclear reaction. This is in good agreement with the spin predicted from log *ft* values.

d. The 1744.5-keV Level. The energy of the 1745-keV level seen by Hinrichsen, Shafroth, and Van Patter[27] corresponds to that of the

1744.5-keV gamma ray determined here. Therefore, this gamma ray must decay to the ground state. The log *ft* of 8.4 for decay to this state corresponds to a first forbidden (unique) beta transition with a spin change of 2 and a parity change, suggesting a $5/2^-$ spin. This is confirmed by an E2 gamma-ray transition to the ground state.

e. The 2633.1-, 2566.5-, and 2530.0-keV Levels. These levels were suggested from the $^{89}Y(p,p')$ nuclear reaction work of Hinrichsen, Shafroth, and Van Patter.[27] The 1712.9-, 1657.3-, and 1620.8-keV gamma rays are probably transitions to the 909.2-keV level from levels at 2622.1, 2566.5, and 2530.0 keV, respectively.

f. The 2.86- and 3.09-MeV Levels. Buchanan, et al.[28] assigned spin $3/2^-$ to levels at 2.86 and 3.09 MeV from their work on the $^{89}Y(n,n'\gamma)$ reaction. These levels should have been fed by electron capture from the $^{89}Zr^m$ level at $1/2^-$, but no peaks were seen at these energies. An upper limit of < 0.015 per cent of all disintegrations was established for the intensity of electron capture branches to levels at 2.86 and 3.09 MeV. This limit corresponds to an estimate of log *ft* > 5.2 for these transitions. This value is still within the limits of an allowed transition and suggests that our experiments may not have been sensitive enough to see these gamma rays.

B. THE DECAY OF NIOBIUM-89 AND NIOBIUM-89m

1. Previous Work

The isomers of ^{89}Nb and $^{89}Nb^m$ were reported by Diamond[29] and by

Mathur, et al.[30] Diamond bombarded niobium foils with 60-MeV protons to make ^{89}Nb and $^{89}Nb^{m}$ from the reaction $^{93}Nb(p,p4n)^{89}Nb$. The activity was followed with a NaI well-type scintillation detector. Diamond was able to resolve three components from the decay curve: a 14.7-hr activity from ^{90}Nb, and 1.9- and 0.8-hr activities from ^{89}Nb. Positron measurements made from an aluminum absorption curve revealed a 2.9-MeV positron that decayed with a 1.9-hr half-life. Likewise, Mathur, et al.[30] bombarded niobium foil with 40-MeV protons to obtain ^{89}Nb and $^{89}Nb^{m}$ activities. Their NaI studies revealed that a 588-keV gamma ray was emitted from $^{89}Nb^{m}$, but no gamma rays were emitted from ^{89}Nb. With an anthracene detector they were able to measure two positrons whose energies were 2.3 MeV and 2.85 ± 0.1 MeV.

Hyde and Nitschke[31] used the reaction $^{81}Br(^{12}C,4n)^{89}Nb$ to make ^{89}Nb activity. Their measurements with Ge(Li) detectors revealed a large number of energetic gamma rays from 1.5 to 3.9 MeV. There was no attempt to establish a decay scheme.

Hanser and Flegenheimer[32] measured the decay of $^{89}Nb^{m}$ by following the half-life of the conversion electrons from the 588-keV transition with a surface barrier detector. They established a half-life of 66 ± 4 min for $^{89}Nb^{m}$.

To resolve this discrepancy and to investigate further the gamma rays from ^{89}Nb, a thorough investigation was made of the positrons and gamma rays from both isomers.

2. Gamma-Ray Singles Spectra

The ^{89}Nb activity was made in this study by bombarding zirconium

oxide, enriched in ^{90}Zr, with 2 μA of 27-MeV protons for 20 minutes. The chemical separation was described in Chapter II. Preliminary single-detector measurements (singles) were made by using a Ge(Li) detector of 20 cm^3 active volume and the SCIPP and 3-D analyzers. These measurements revealed many high-energy gamma rays of low intensity. Final singles measurements were made with a 35 cm^3 Ge(Li) detector and a 4096-channel analyzer. Figure 11a shows a normal low-energy spectrum of ^{89}Nb and $^{89}Nb^m$.

To obtain good counting statistics for the high-energy, low-intensity gamma-ray peak, a high counting rate is needed. However, high counting rates tend to degrade the resolution. To keep the counting rate low, yet obtain good statistics for the high-energy gamma rays, the sample was counted through 1.5 cm of lead. Lead decreases the intensity of the low-energy gamma rays. The spectra shown in Figures 11b and 12 were obtained by counting gamma rays from the ^{89}Nb source through lead. A correction for the lead attenuation was made before the intensities of the gamma rays were computed.

To confirm that these gamma rays were from ^{89}Nb and $^{89}Nb^m$, the ion exchange column (c.f., Chapter II) was counted 2 min after zirconium separation, and the 588-keV gamma rays were counted for short periods of time using 400 channel subgroups of the memory of the SCIPP analyzer to store the data. The growth and decay of the 588-keV peak shows 5.6 ± 2.0 and 69.5 ± 2.0 min components, as shown in Figure 13. The 5.6- min growth of the 588-keV activity, characteristic of $^{89}Zr^m$, identifies the niobium mass as 89. The 70-min half-life corresponds to the half-life

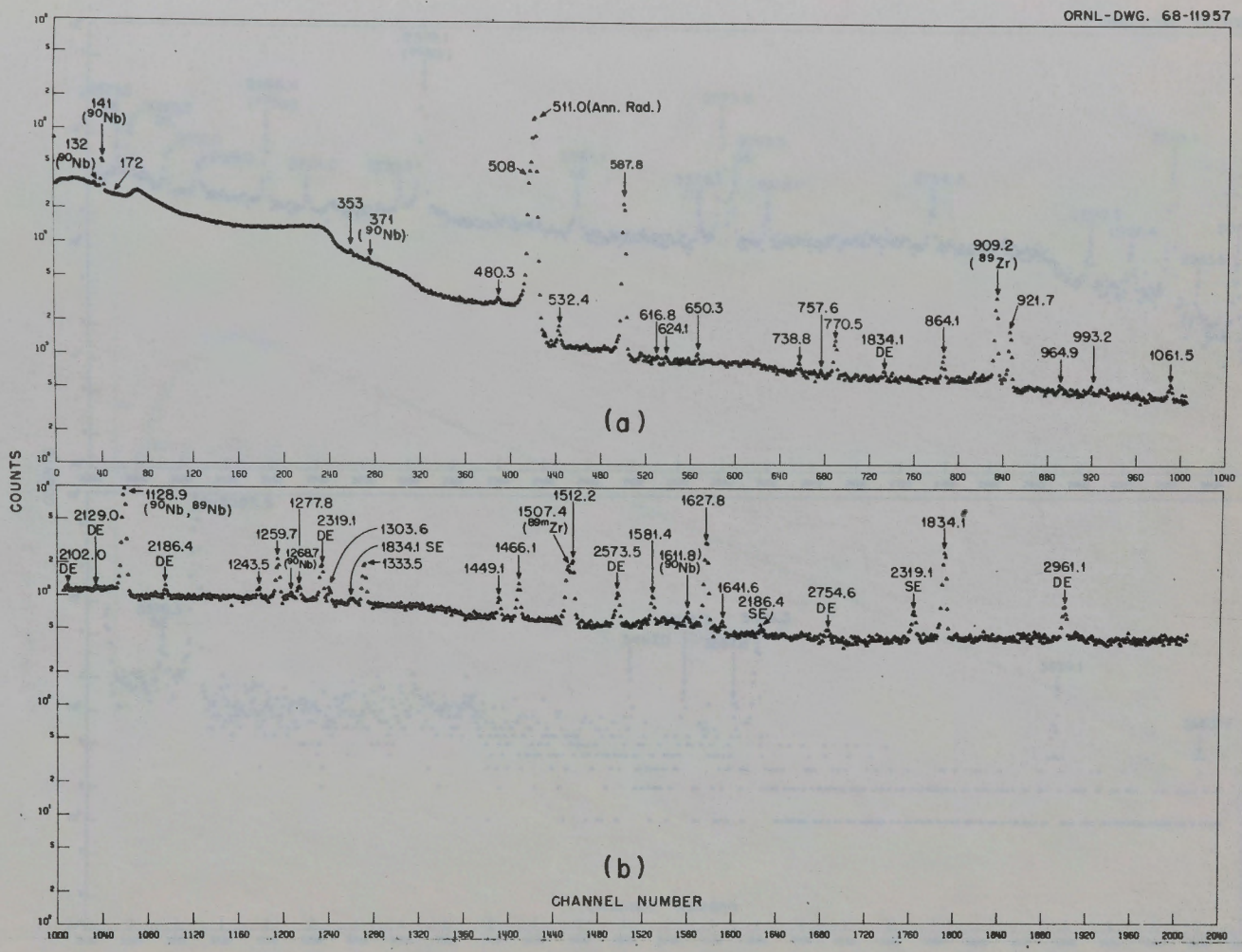


Figure 11. The low-energy portion of the ^{89}Nb gamma ray spectrum taken with a 35 cm^3 Ge(Li) detector. The spectrum in part (a) was not counted through lead. The spectrum in part (b) was counted through 1.5 cm of lead.

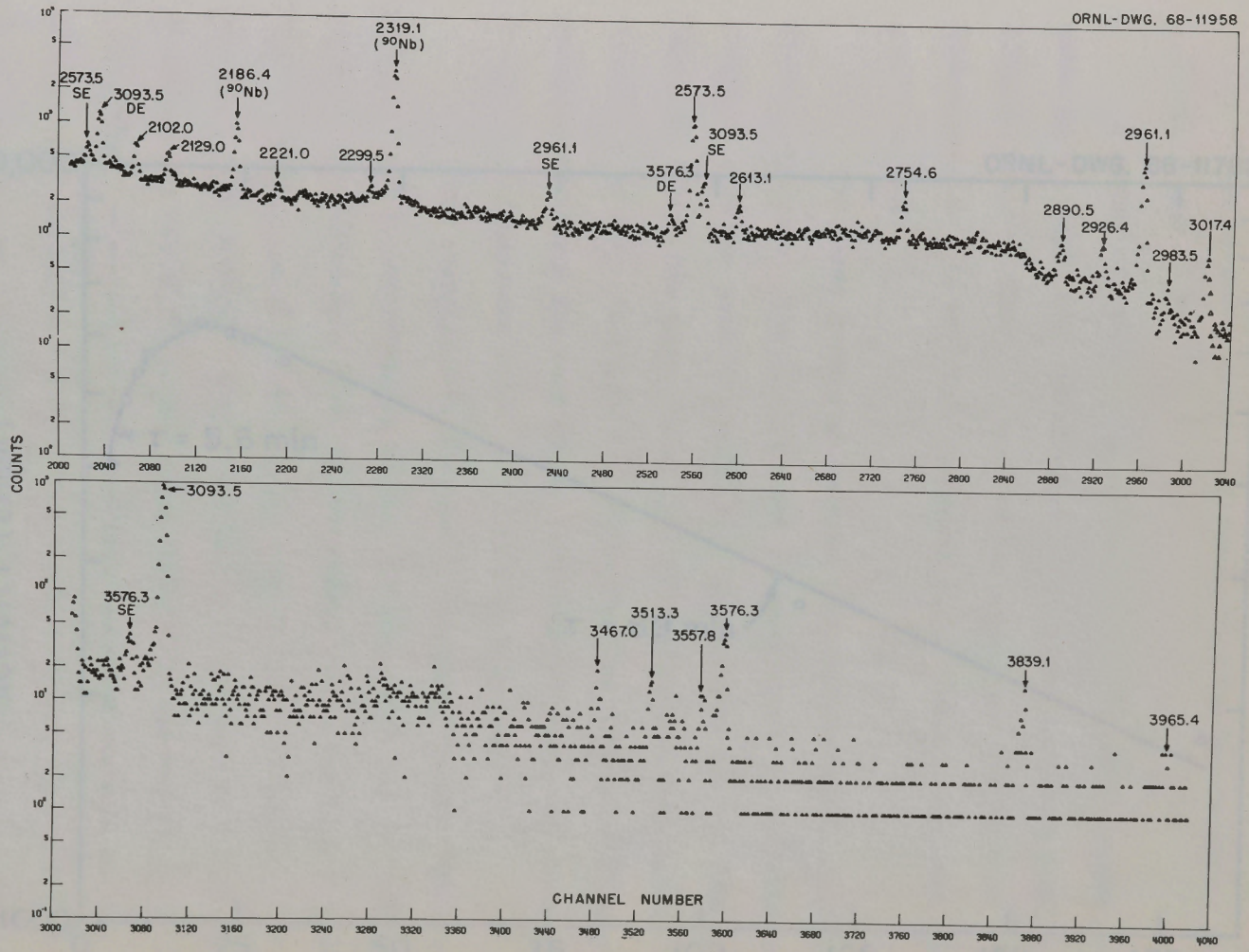


Figure 12. The high-energy portion of the ^{89}Nb gamma-ray spectrum taken with a 35 cm^3 Ge(Li) detector by counting through 1.5 cm of lead. Energies are in keV. Single and double escape peaks are represented respectively as SE and DE.

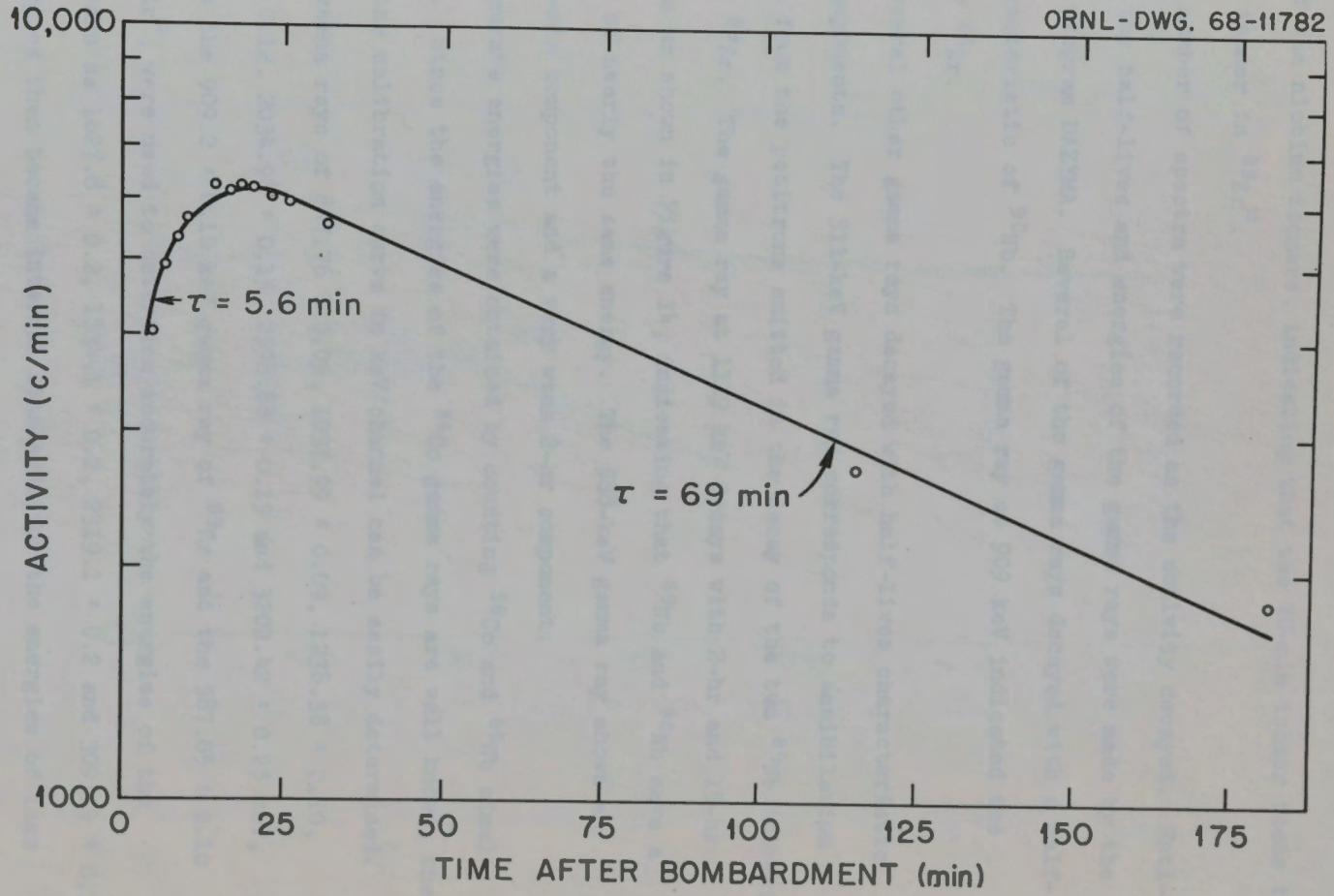


Figure 13. The growth and decay of the 588-keV gamma-ray counted 2 minutes after a zirconium separation.

of one of the niobium isomers, indicating that the 70-min isomer feeds the 4.16-min isomer in $^{89}Zr^{m}$.

A number of spectra were recorded as the activity decayed. Estimates of the half-lives and energies of the gamma rays were made by the computer program DAZYMA. Several of the gamma rays decayed with a half-life characteristic of ^{90}Nb. The gamma ray at 909 keV indicated the growth of ^{89}Zr.

Several other gamma rays decayed with half-lives characteristic of two components. The 511-keV gamma ray corresponds to annihilation radiation from the positrons emitted in the decay of the two ^{89}Nb isomers, ^{90}Nb, and ^{89}Zr. The gamma ray at 1129 keV decays with 2-hr and 15-hr half-lives as shown in Figure 14, indicating that ^{89}Nb and ^{90}Nb have a gamma ray of nearly the same energy. The 588-keV gamma ray shows a strong 70-min component and a very weak 2-hr component.

Accurate energies were obtained by counting ^{56}Co and ^{89}Nb simultaneously. Since the energies of the ^{56}Co gamma rays are well known, the slope of the calibration curve in keV/channel can be easily determined. The ^{56}Co gamma rays of 847.76 ± 0.09, 1037.99 ± 0.09, 1238.38 ± 0.10, 1771.74 ± 0.12, 2034.98 ± 0.15, 2598.88 ± 0.15 and 3202.42 ± 0.25 keV, as well as the 909.2 ± 0.10 keV gamma ray of ^{89}Zr and the 587.85 ± 0.10 keV of $^{89}Zr^{m}$, were used to determine accurately the energies of the intense peaks as 1627.8 ± 0.2, 1834.1 ± 0.2, 2319.1 ± 0.2 and 3093.4 ± 0.3. These energies then became internal standards for the energies of less intense peaks. The intensities of the gamma rays were determined by dividing the area of the peaks by the detector efficiency. Gamma-ray

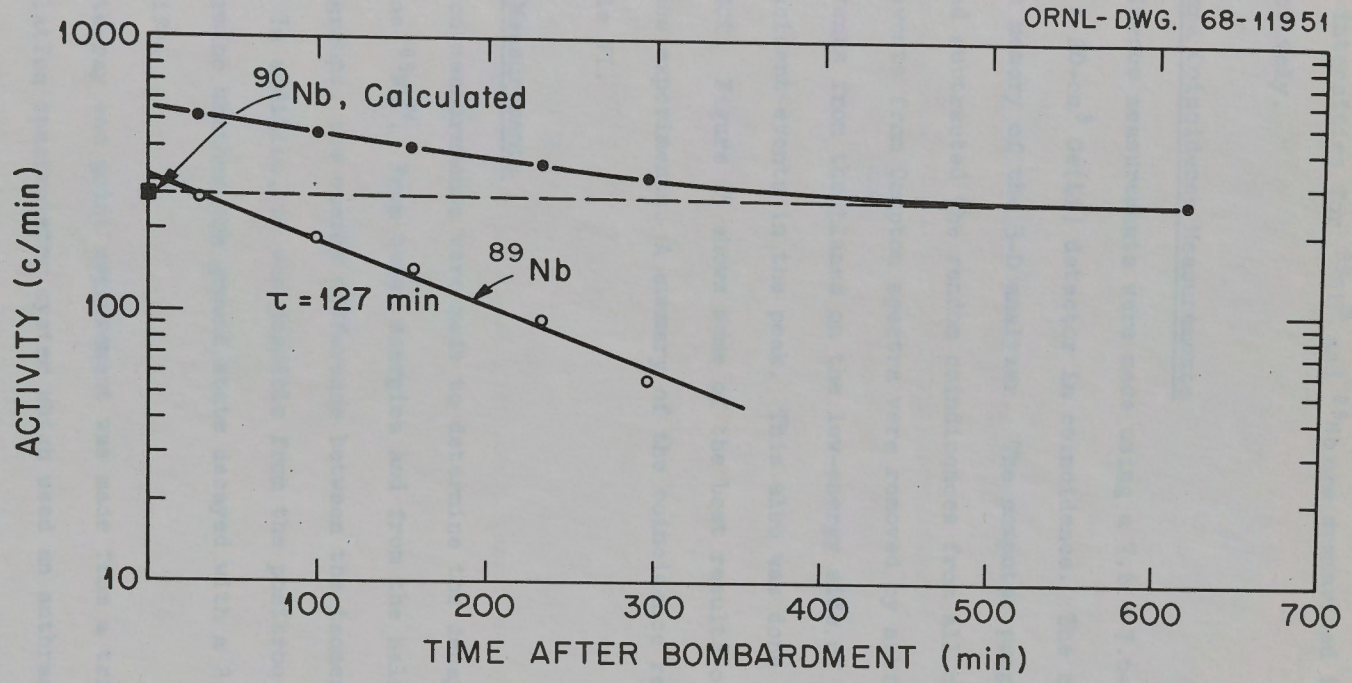


Figure 14. The decay of the 1129-keV gamma-ray showing ^{90}Nb and ^{89}Nb components.

energies and intensities for $^{89}Nb^{m}$ and ^{89}Nb are summarized in Tables IV and V, respectively.

3. Gamma-Gamma Coincidence Measurements

Coincidence measurements were made using a 7.6 × 7.6-cm NaI detector and a 20-cm^3 Ge(Li) detector in coincidence. The counts were stored in the memory of the 3-D analyzer. The computer program KORRECT calculated and subtracted the random coindicences from all counts. Coincident events from Compton spectra were removed by subtracting the coincident events from the planes on the low-energy side of the peak from the coincident events in the peak. This also was done by using program KORRECT. Figure 15 shows some of the best results obtained from the coincidence experiments. A summary of the coincidence results is given in Table VI.

4. Positron Measurements

Positron measurements were made to determine the decay energy of ^{89}Nb as well as $^{89}Nb^{m}$. From these energies and from the half-life of the positron groups, the energy difference between the isomers can be established. In addition, it was possible from the positron measurements to determine whether the ground state decayed with a 2-hr or a 70-min half-life.

The beta-ray end point measurement was made from a triple coincidence scintillation spectrometer system which used an anthracene crystal and two NaI crystals, as described earlier in Chapter II. A beta-ray distribution was measured on the SCIPP analyzer. The 624-keV and 975-keV

TABLE IV

SUMMARY OF THE $^{89}Nb^{m}$ GAMMA-RAY RESULTS

E_γ (keV)	Relative Intensity
508	80 ±20
587.85 ± 0.15	100
650.3 ± 0.8	0.75 ± 0.9
770.5 ± 0.6	4.6 ± 0.5
1277.8 ± 0.4	1.4 ± 0.1

TABLE V

SUMMARY OF THE ^{89}Nb GAMMA-RAY RESULTS

This Work		Hyde and Nitsche[31]
E_γ (keV)	Relative Intensity	E_γ (keV)
172 ± 2	1.8 ± 1.5	
356 ± 2	10 ± 5	
480.3 ± 0.7	8 ± 1	
508 ± 1	28[a]	
532.4 ± 0.7	18 ± 2	
587.85 ± 0.15	46[a]	
616.8 ± 1.0	2.0 ± 0.8	
624.1 ± 0.7	3.2 ± 1.0	
738.8 ± 0.7	6.5 ± 0.6	
757.6 ± 0.7	2 ± 2	
864.1 ± 0.3	18 ± 2	
921.7 ± 0.3	46 ± 5	
964.9 ± 0.6	5.3 ± 0.6	
993.2 ± 0.6[b]	5.7 ± 0.6	
1061.4 ± 0.4	9.5 ± 1.0	
1129 ± 1	55 ±10	
1243.5 ± 0.6	5.6 ± 0.7	
1259.7 ± 0.3	35 ± 4	

TABLE V (continued)

This Work		Hyde and Nitsche[31]
E_γ (keV)	Relative Intensity	E_γ (keV)
1303.6 ± 0.5	11 ± 1	
1333.5 ± 0.3	35 ± 4	
1449.1 ± 0.4	8.9 ± 1.0	
1466.1 ± 0.3	23 ± 2	
1512.2 ± 0.5	53 ± 6	1510 ± 5
1581.4 ± 0.4	14 ± 2	
1627.8 ± 0.2	100 ±	1626 ± 5
1641.6 ± 0.7	5.9 ± 0.6	
1834.1 ± 0.2	90 ± 9	1832 ± 5
2102.0 ± 0.5	15 ± 2	
2129.0 ± 0.6	14 ± 2	
2221.0 ± 0.5	5.2 ± 0.6	2220 ± 5
2299.5 ± 0.6	1.4 ± 1.0	
2573.5 ± 0.4	79 ± 8	2572 ± 1
2613.1 ± 0.4	7.5 ± 0.8	
2754.6 ± 0.4	11 ± 1	2754 ± 1
2890.5 ± 0.6	5.6 ± 0.6	
2926.4 ± 0.5	6.7 ± 0.7	
2961.1 ± 0.4	46 ± 5	2961 ± 1

TABLE V (continued)

This Work		Hyde and Nitsche[31]
E_γ (keV)	Relative Intensity	E_γ (keV)
2983.5 ± 0.8	2.2 ± 0.2	
3017.4 ± 0.5	5.6 ± 0.6	3018 ± 1
3093.5 ± 0.3	8.6 ± 8	3093 ± 1
3467.0 ± 1.0	1.1 ± 0.3	
3513.3 ± 0.8	1.3 ± 0.3	3513 ± 1
3557.8 ± 0.8	1.4 ± 0.3	3577 ± 1
3576.3 ± 0.7	4.8 ± 0.5	
3839.1 ± 1.0	0.91 ± 0.10	3838 ± 1
3965.4 ± 1.5	0.2 ± 0.1	

[a]Value inferred from decay scheme.

[b]Not placed in decay scheme.

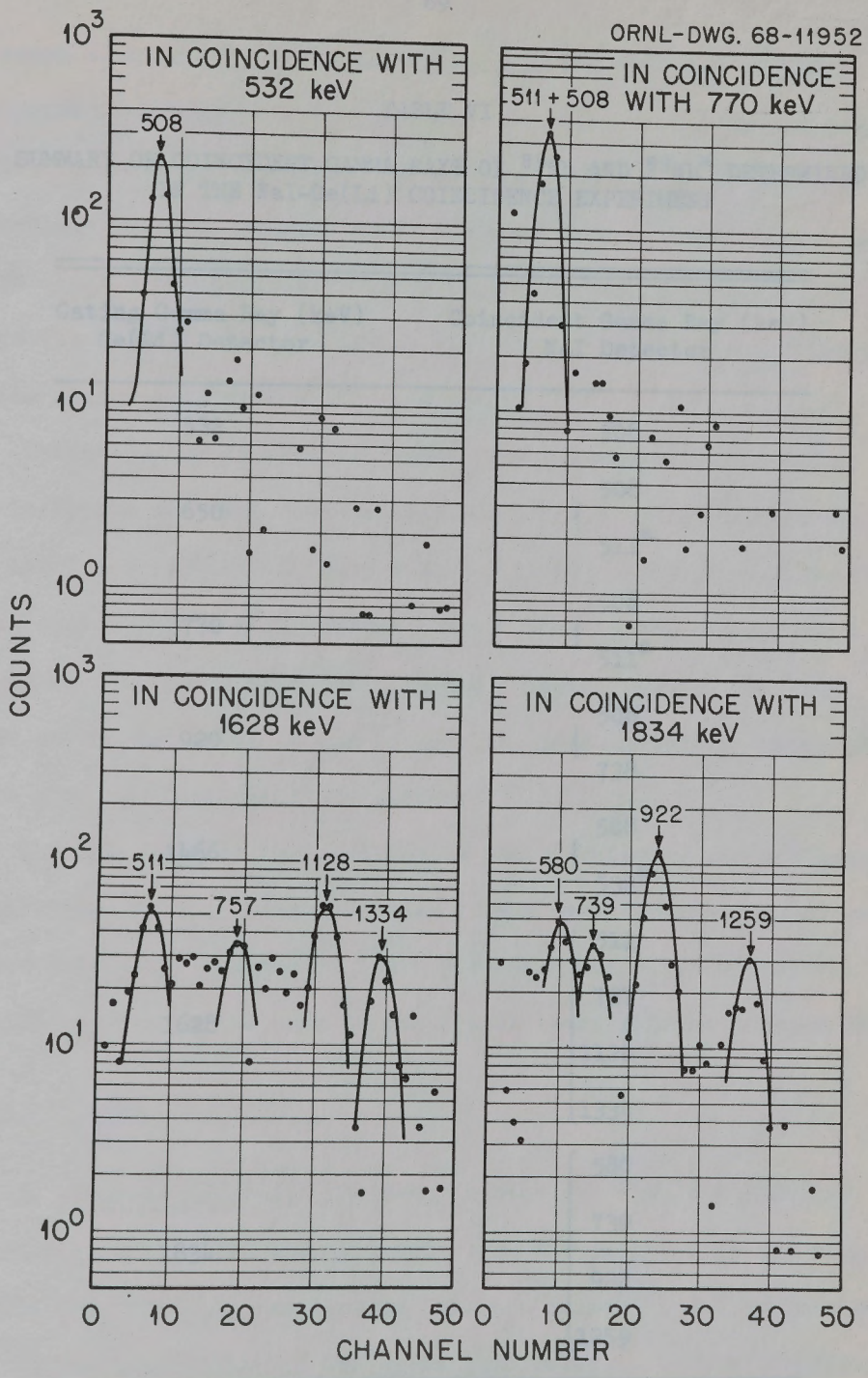


Figure 15. Gamma-ray spectrum (NaI) of ^{89}Nb in coincidence with gamma rays counted with a Ge(Li) detector.

TABLE VI

SUMMARY OF COINCIDENT GAMMA RAYS OF ^{89}Nb AND $^{89}Nb^{m}$ DETERMINED IN THE NaI-Ge(Li) COINCIDENCE EXPERIMENT

Gating Gamma Ray (keV) Ge(Li) Detector	Coincident Gamma Ray (keV) NaI Detector
532	508
650	508
	511[a]
770	508
	511[a]
920	508
	738
1466	508
	532[a]
1628	511
	757
	1128
	1334
1834	580
	739
	922
	1259

[a]Unresolved with the 508-keV gamma ray.

conversion electrons of ^{137}Cs and ^{207}Bi, and the 3000-keV end point of ^{144}Pr provided energy calibrations. In addition, when ^{89}Nb had decayed away the 1500-keV end point of ^{90}Nb provided a calibration point of intermediate energy. Program KURIE was used to make Fermi-Kurie plots from the beta distributions. The end point was found by drawing a line through the straight portion of the plot. The intersection of the line with the energy axis defines the end point.

Three components were extracted from the Fermi-Kurie plot as shown in Figure 16. The beta-ray end point energies for components, 1, 2, and 3 are 3.34 ± 0.10 MeV, 2.82 ± 0.12 MeV and 2.38 ± 0.15 MeV respectively. The largest factors contributing to the energy error are calibration, end point extrapolation and detector resolution. The scatter at the end point is due to detector pile-up pulses, which give rise to spurious high-amplitude pulses.

The half-life of the spectrum in the vicinity of the end point was determined by following the decay of the beta distribution between 2.82 and 3.34 MeV. A value of 125 ± 3 minutes was obtained for the half-life by fitting the data to the linear least squares program FRANTIC.

5. Decay Scheme

1. General Remarks. The decay scheme for ^{89}Nb and $^{89}Nb^{m}$ is shown in Figure 17. The energy levels were determined with the help of data from the $^{90}Zr(p,d)$ reaction by Ball and Fulmer[33], and by Taketani, et al.[34] The intensities of the gamma rays relative to the intensity of the 1627.8-keV gamma ray are indicated in italics. The energy sums

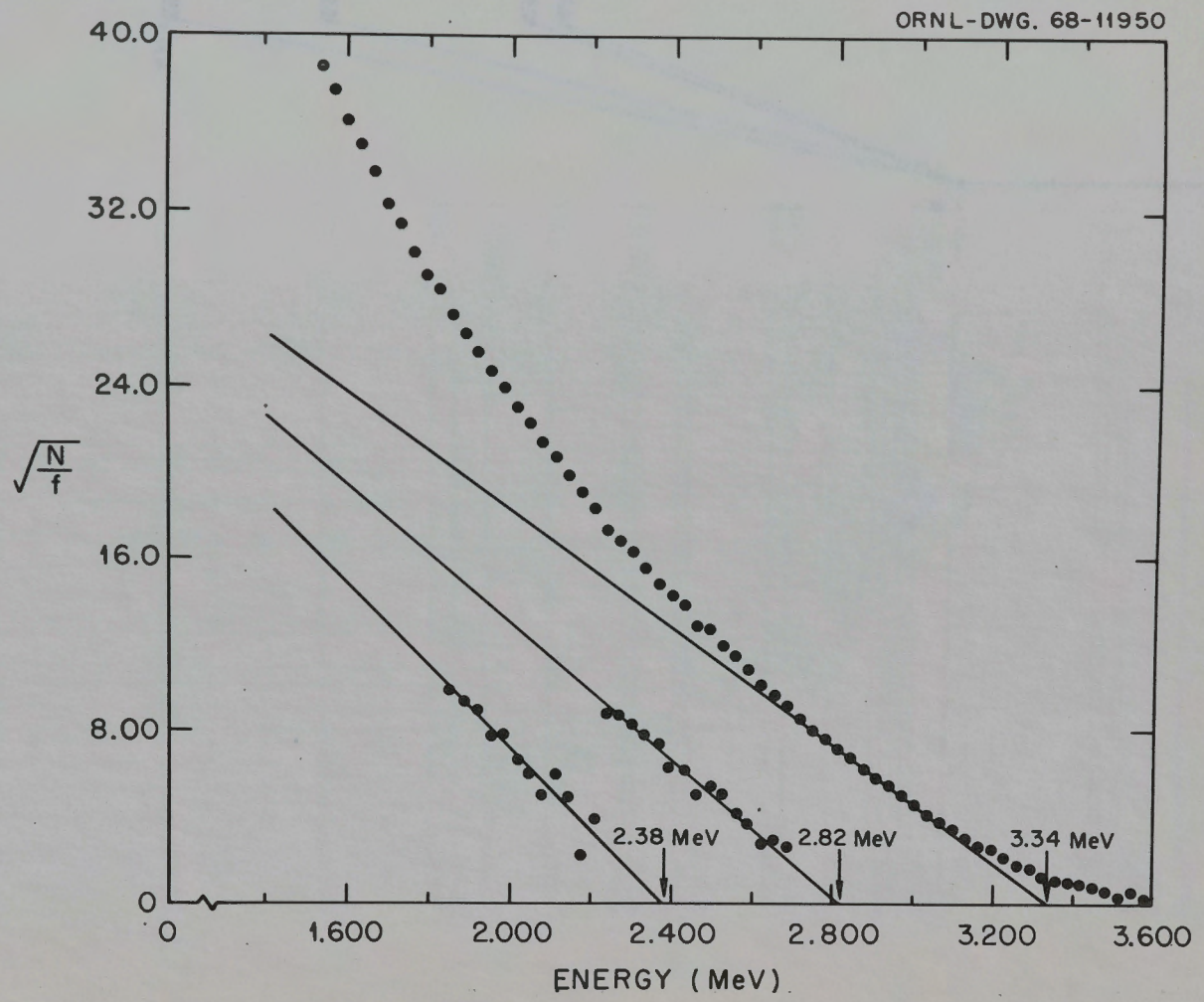


Figure 16. Fermi analysis of the positron spectrum of ^{89}Nb and $^{89}Nb^{m}$.

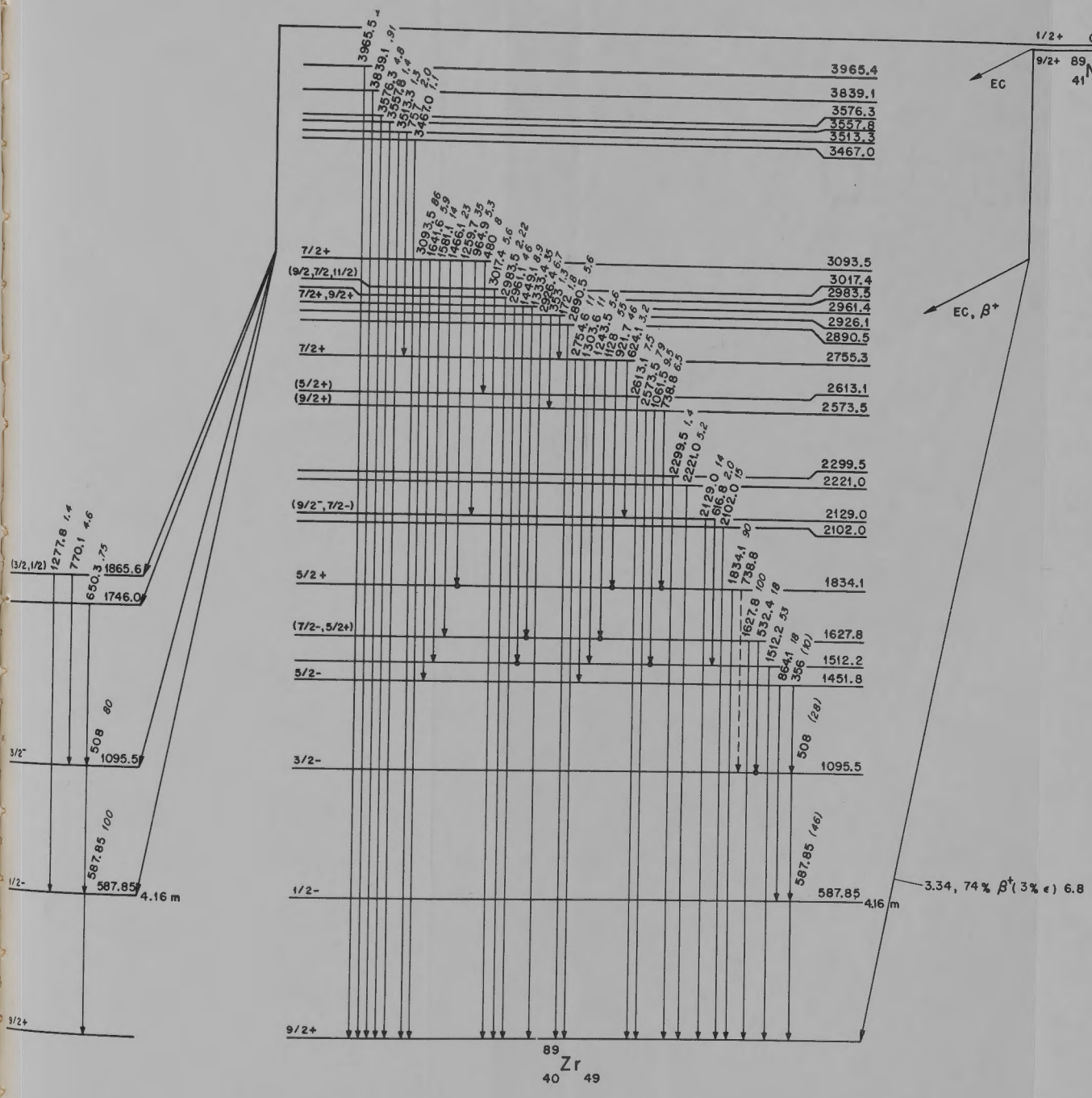


Figure 17. Decay scheme proposed for ^{89}Nb and $^{89}Nb^{m}$.

of all cascade transitions agree in most cases to within 0.6 keV. An exception occurs at the 2755.3-keV level. The energy difference between the 2755.3- and 2129.0-keV levels is 626.3 keV, 2.2 keV greater than the 624.1-keV gamma ray indicated on the decay scheme. Also, the cross-over transition represented by the 2754.6-keV gamma ray is 0.7 keV less than the energy of the level calculated from the sums of coincident gamma rays. The shape of the 2754.6-keV gamma-ray peak suggests the possibility of a doublet at this energy.

Uncertain transitions are indicated with dotted lines. The 738.8-keV transition between the levels at 1834.1 and 1095.5 keV was suggested, because the coincidence data hinted that the 1127.5- and 1259.7-keV gamma rays were in coincidence with the 738-keV gamma ray. Yet the gamma-ray intensities feeding the 1834.1-keV level equal the intensity depopulating the level without including the intensity of the 738-keV gamma ray. There seems to be a coincidence between the 1834.1-keV gamma ray and the 738.8-keV gamma ray. Perhaps there are two gamma rays at about 738 keV. If this is the case, one 738-keV gamma ray may decay to the level and another 738-keV gamma ray may depopulate it.

There are uncertainties regarding transitions to the 1627.8- and 1512.2-keV levels. Coincidence data indicate that a gamma ray of about 511 keV is in coincidence with 1627.8 keV, which suggests positron decay to the level. However, the total intensity of gamma rays decaying into the level nearly equals the total intensity of gamma rays leaving the level without any indication of positron transitions to the level. The 1512-keV gamma ray also indicates 511-keV coincident events. However,

in the coincidence experiment, the 1508-keV gamma ray from $^{89}Zr^{m}$ and the 1512-keV gamma rays of ^{89}Nb are not resolved. The decay scheme shown in Figure 10 proposes that the 1508-keV level in ^{89}Y is populated partially by positron decay of $^{89}Zr^{m}$.

The intensities of the 508-keV gamma ray and the 587.8-keV gamma ray from the decay of 125-min ^{89}Nb shown in the decay scheme are calculated from the intensities of the gamma rays feeding the level which they depopulate. They are much weaker than the 508- and 587.8-keV gamma rays from the positron decay of 70-min $^{89}Nb^{m}$ and cannot easily be resolved in a two-component decay analysis. The 508-keV gamma ray is not easily seen in Figure 11a. However, in other spectra the hump on the low-energy side of the positron annihilation peak at 511 keV is quite pronounced.

2. Beta Transitions. The ground state of $^{89}_{41}Nb_{48}$ is $9/2^{+}$, since the 41st proton must be in the $g_{9/2}$ shell. The ground state of $^{89}_{40}Zr_{49}$ is also $9/2^{+}$, so a beta transition between the ground states is expected. The 3.34-MeV positron is assigned to this transition. The energy difference between the ground states (Q-value) is 3.34 + 1.02, or 4.36 MeV.

The first excited state of ^{89}Nb is predicted to be $1/2^{-}$, which corresponds to decoupling a $p_{1/2}$ proton from the other $p_{1/2}$ proton, promoting a $p_{1/2}$ proton to the $g_{9/2}$ level, where it couples with the long $g_{9/2}$ proton. The proton hole in the $p_{1/2}$ level determines the spin of $1/2^{-}$. One then expects a positron transition between $^{89}Nb^{m}$ and $^{89}Zr^{m}$. Experimentally, the 588-keV gamma ray is very intense. The

2.82-MeV positron group is the transition from $^{89}Nb^{m}$ to the $1/2^{-}$ level of ^{89}Zr at 588 keV. The energy difference between zirconium and niobium isomer levels is 2.82 + 1.02 or 3.84 MeV. Since it decays to a level 0.59 MeV above the ^{89}Zr ground state, the energy difference between the ground state and $^{89}Nb^{m}$ is 4.43 MeV. Therefore, the isomeric state, $^{89}Nb^{m}$, is about 70 keV above the ^{89}Nb ground state. From the decay scheme shown in Figure 17 it can be seen that the remaining positrons must feed the 1095.5-keV level from the decay of $^{89}Nb^{m}$, since the 508-keV gamma ray is strong.

The 511-keV peak contains contributions from the 508-keV gamma ray and the positron annihilation radiation from the decays of ^{90}Nb, ^{89}Nb, $^{89}Nb^{m}$, and ^{89}Zr. To determine the per cent of disintegrations decaying from ^{89}Nb to the ground state of ^{89}Zr, annihilation radiation from all the other isotopes must be subtracted, as well as the area due to the 508-keV gamma ray. The 2319-keV gamma ray was used to determine the ^{90}Nb contribution. In a similar manner, the 909-keV gamma ray represents the amount of ^{89}Zr daughter formed. The positrons feeding the 1095.5- and 587.8-keV levels from the decay of $^{89}Nb^{m}$ were estimated from the 587.8- and 508-keV gamma-ray intensities. Most of the remaining annihilation radiation peak area represents positron decay to the ground state of ^{89}Zr. A small percentage of positrons decay to excited states of ^{89}Zr. The number of positron decays exciting each level corresponds to the difference between the gamma-ray intensity feeding a level and the gamma-ray intensity depopulating the level. This difference must be corrected for electron capture, since the

higher-energy excited states are fed mostly by electron capture. The total number of disintegrations is the sum of the positrons decaying to the ground state, the positron transitions to excited states and electron capture decays to these excited states and to the ground state. By dividing the number of positrons decaying to the ground state by the total number of disintegrations, a ground state percentage of 74 was obtained. The percentage of positron decay and electron capture to each excited state was calculated in a similar manner. The log *ft* values were then calculated for each level excited by positron decay or electron capture and are shown on Table VII.

3. The 587.8-keV Level. The 4.16-min half-life of this level corresponds to an M4 transition. The log *ft* value is consistent with an allowed transition, i.e., a spin change of 0 or 1 with no parity change. On this basis, a $1/2^-$ spin assignment was made for this level. The results of nuclear reaction work support this assignment.

4. The 1095.5-keV Level. This level is intensely excited in the decay of $^{89}Nb^m$. The relatively low log *ft* value is consistent with a spin change of 0 or 1 and no parity change, which is consistent with a spin of $3/2^-$ or $1/2^-$ for the level.

5. The 1746.0- and 1865.6-keV Levels. The low log *ft* value indicates a spin change of 0 or 1 with no parity change. Therefore, the spins of these levels are either $3/2^-$ or $1/2^-$.

6. The 1451.8-keV Level. There is a strong gamma-ray transition

TABLE VII

VALUES[a] OF LOG *ft* FOR BETA TRANSITIONS IN THE DECAY OF ^{89}Nb AND $^{89}Nb^{m}$

Level	Beta (or Electron Capture) Energy	% β	% ε	Log *ft*
Ground State	3.34	74	(3)	6.8
588.85	2.82	(18	1.2	6.0)
1095.5	2.38	(67	8	6.8)
1746.0	(1.66	0.58	0.17	7.2)
1865.6	(1.54	4.6	1.7	5.8)
2129.0	(1.24	0.31	0.31	7.3)
2221.0	(1.12	0.08	0.13	7.5)
2299.5	(1.04	0.02	0.04	8.0)
2573.5	(0.77	0.7	3.1	5.9)
2755.3	(0.58	0.35	5.2	5.5)
2890.5	(0.45	0.006	0.27	6.7)
2926.1	(0.41	0.007	0.40	6.6)
2961.4	(0.38	0.06	3.6	5.7)
2983.5	(0.36	0.008	0.087	7.2)
3017.4	(0.32	0.8×10^{-3}	0.24	7.8)
3093.5	(0.25	0.02	7.1	5.2)
3467.0	(0.89		0.64	7.2)
3513.3	(0.85		0.12	6.5)
3557.8	(0.80		0.12	6.6)

TABLE VII (continued)

Level	Beta (or Electron Capture) Energy	% β	% ε	Log *ft*
3576.3	(0.78		0.20	6.3)
3839.1	(0.52		0.04	6.7)
3965.5	(0.39		0.01	7.1)

[a]Values in parenthesis were computed, not measured directly.

to the 588-keV level. Since the favored gamma-ray transitions are M1, E1, or E2, the possible spins for this level are $1/2^-$, $1/2^+$, $3/2^-$, $3/2^+$, $5/2^-$. Coincidence data show that there is no 511-keV radiation in coincidence with the 864-keV gamma ray. The spin change for decay from the $1/2^-$ isomer of ^{89}Nb must be less than 2 for beta decay to this level. A spin of $5/2^-$ is the assignment.

7. The 1834.1-keV Level. There are no 511-keV gamma rays in coincidence with the 1834-keV gamma ray. Therefore, there is no detectable positron decay to this level, and so the spin change for positron decay from the $9/2^+$ ground state of ^{89}Nb must be 2 or greater. Since gamma decay is observed to the $9/2^+$ ground state of ^{89}Zr, the spin change to the $9/2^+$ ground state cannot be greater than 2 with no parity change. The spin of the 1834-keV level then must be either $5/2^+$ or $13/2^+$. A possible E1 transition to the 1095.6-keV level would support the $5/2^+$ assignment for the 1834-keV level and the $3/2^-$ assignment for the 1095.5-keV level. A gamma ray has been seen at 738.8 keV which has been tentatively identified as this E1 transition.

8. The 2754.6- and 3093.5-keV Levels. The low values of log *ft* for beta decay to the 2755- and 3093.5-keV levels suggest spin changes of 0 or 1 with no parity change, for transitions to these levels. Possible spins of the levels are $9/2^+$, $11/2^+$, or $7/2^+$. Gamma-ray transitions are seen from each of these levels to the $5/2^-$ level at 1451 keV. These transitions are most likely E1, which is consistent only with an assignment of $7/2^+$ to both levels.

9. The 1627.8-keV level. It is uncertain that the 1627.8-keV level is populated either by positron decay or by electron capture. Since there is a positron transition to the $9/2^+$ ground state the spin is $9/2 \pm 2$. Spins within both boundaries are $(7/2, 5/2)^{\pm}$. A $5/2^-$ spin is eliminated as a possibility, since an M2 gamma-ray transition to the ground state would be highly unlikely. In a similar manner the $7/2^+$ assignment must be eliminated, because the 532.7-keV gamma-ray transition between the 1627.8- and 1095.5-keV levels would be M2 and so would be too weak to be seen. The remaining possible spins are $7/2^-$ and $5/2^+$. Either of these assignments are consistent with a spin assignment of $3/2^-$ for the 1095.5-keV level, because the 532.7-keV gamma-ray transition would be E2 or E1, in qualitative agreement with the gamma intensity determined in this study.

10. The 2961.4-keV level. The low value of log *ft* suggests a spin change of 0 to 1 and no parity change. The possible spins are $11/2^+$, $9/2^+$, $7/2^+$. A gamma-ray transition to the 1627.8-keV level eliminates the $11/2^+$ spin, since the highest possible spin for this level is $7/2^-$, and M2 transitions are improbable.

11. The 3017.4-keV level. The high value of log *ft* for decay to this level is characteristic of a first-forbidden positron transition, which corresponds to a spin change of 0 or 1 with a parity change. Possible spins are $11/2^-$, $9/2^-$, and $7/2^-$ for this level.

12. The 2573.5-keV level. An allowed transition from ^{89}Nb to this state is suggested by the low value of log *ft*. Therefore, possible

spin assignments for the 2573-keV level are $11/2^+$, $9/2^+$, $7/2^+$. A gamma-ray transition to the $5/2^+$ level at 1451.8 keV eliminates $11/2^+$. The absence of an E1 transition from the 2573.5-keV level to the 1451.8-keV state eliminates a $7/2^+$ spin assignment for this state. The remaining possibility is $9/2^+$, as shown in the decay scheme.

13. The 2129.0-keV level. The value of log *ft* for the positron transition to this level suggests a spin change of 0 or 1 and a parity change. Possible assignments are $11/2^-$, $9/2^-$, and $7/2^-$. Gamma-ray transitions from $7/2^+$ levels at 2755.3 and 3093.5 keV eliminate the $11/2^-$ possibility, so only $9/2^-$ and $7/2^-$ remain.

The difference between the gamma-ray intensity exciting a level and that depopulating a level is assumed to be made up by positrons or electron capture. However, gamma-ray transitions into the remaining levels were too weak to be seen. There, the log *ft* values assigned to these levels may be too low.

The first excited states determined from this experiment are in good agreement with work on the $^{90}Zr(p,d)^{89}Zr$ reaction by Ball and Fulmer,[33] and by Taketani, et al.[34] Some levels are fed by beta decay which are not seen in the (p,d) reaction work, and *vice-versa*. The levels seen in this work are compared in Figure 18 with preliminary calculations by Ball[35] and with experimental data.

14. Half-Lives. The half-life of $^{89}Nb^m$ are determined by following the decay of the 588-keV gamma ray. It can be seen from the

ORNL-DWG. 68-11955

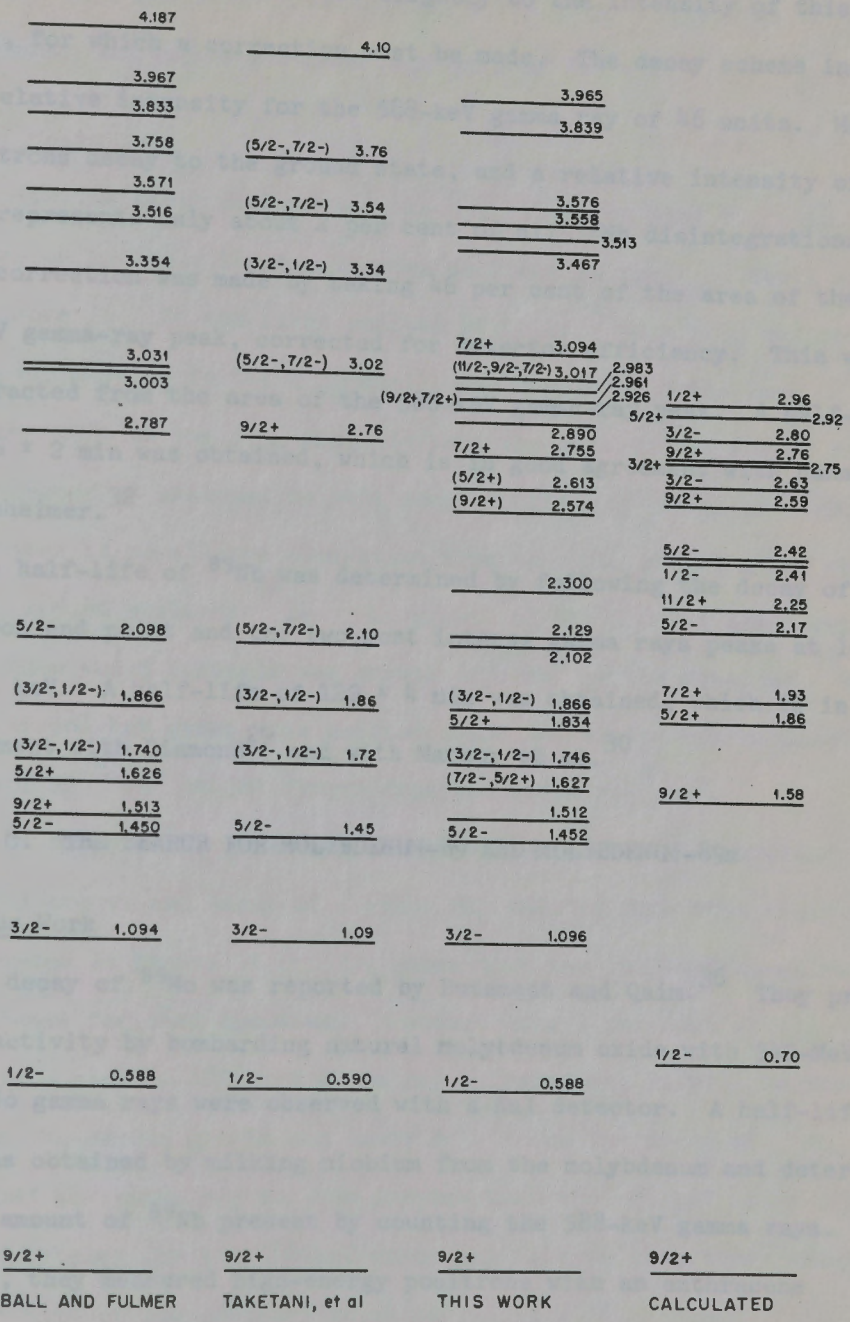


Figure 18. A comparison of the experimental level spectra obtained from the decay of the ^{89}Nb isomers, the ^{90}Zr(p,d) reaction, and the results of the effective interaction method obtained by Ball.

decay scheme that ^{89}Nb contributes slightly to the intensity of this gamma ray, for which a correction must be made. The decay scheme indicates a relative intensity for the 588-keV gamma ray of 46 units. Most ^{89}Nb positrons decay to the ground state, and a relative intensity of 46 units represents only about 2 per cent of all ^{89}Nb disintegrations. The ^{89}Nb correction was made by taking 46 per cent of the area of the 1627.8-keV gamma-ray peak, corrected for detector efficiency. This was then subtracted from the area of the 588-keV gamma-ray peak. A half-life of 66 ± 2 min was obtained, which is in good agreement with Hanser and Flegenheimer.[32]

The half-life of ^{89}Nb was determined by following the decay of the positron end point and the two most intense gamma rays peaks at 1627.8 and 1834.1 keV. A half-life of 122 ± 4 min was obtained, which is in good agreement with Diamond[29] and with Mathur et al.[30]

C. THE SEARCH FOR MOLYBDENUM-89 AND MOLYBDENUM-89m

1. Previous Work

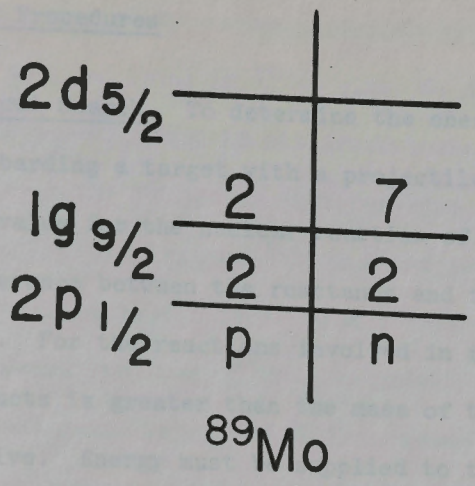
The decay of ^{89}Mo was reported by Butement and Qaim.[36] They produced the activity by bombarding natural molybdenum oxide with 340-MeV protons. No gamma rays were observed with a NaI detector. A half-life of 9 min was obtained by milking niobium from the molybdenum and determining the amount of ^{89}Nb present by counting the 588-keV gamma rays. In addition, they measured high-energy positrons with an anthracene scintillation detector. An energy discriminator was used to bias out the low-energy positrons below 3.6 MeV, since all known molybdenum

isotopes have positrons with energies below this energy. The positrons above 3.6 MeV were observed to decay with a 7-min half-life. On this basis, Butement and Qaim reported a half-life of 7.1 min.

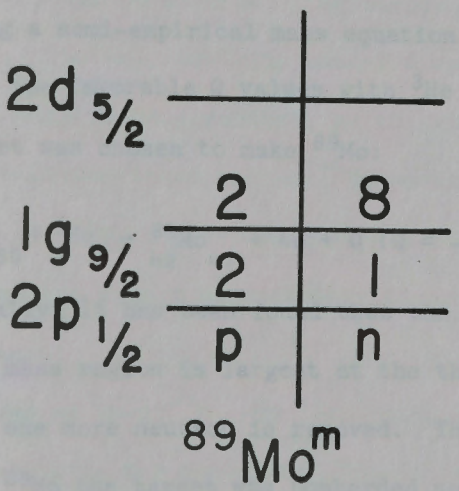
2. Isomer Predictions

As with the other neutron-deficient nuclides of mass 89, $^{89}_{42}Mo_{47}$ probably has an isomer. There are seven neutrons in the $g_{9/2}$ shell as shown in Figure 19. In the first excited state of ^{89}Mo a $p_{1/2}$ neutron will decouple, advance to the $g_{9/2}$ shell, and couple with the lone neutron. The hole in the $p_{1/2}$ shell defines the spin of the isomer as $1/2^-$. The isomer is expected to beta decay to the $1/2^-$ level in ^{89}Nb. Likewise, there is an allowed transition from the $9/2^+$ ground state of ^{89}Mo to the ground state of ^{89}Nb. The growth of the 588-keV gamma ray from $^{89}Zr^m$ then would indicate the growth of $^{89}Nb^m$ or the decay of $^{89}Mo^m$. The number of 588-keV gamma rays emitted would be related approximately to the number of $^{89}Nb^m$ nuclei formed from the decay of $^{89}Mo^m$.

On the other hand, to detect the growth of ^{89}Nb it is necessary to follow the growth and decay of a gamma ray emitted from that nuclide. The decay scheme in Figure 17 (p. 72) shows that the 1627-keV gamma ray is the most intense for that spectrum. However, only 4 per cent of all ^{89}Nb disintegrations yield a 1627-keV gamma ray. Therefore, it will be more difficult to follow the growth and decay of ^{89}Nb or the decay of ^{89}Mo, since the 1627-keV gamma ray is less intense than the 588-keV gamma ray. Also, the efficiency for the 588-keV gamma ray is more than three times greater than that of the 1627-keV gamma ray.



(a)



(b)

Figure 19. Schematic shell-model description of (a) ground state of ^{89}Mo, and (b) $^{89}Mo^{m}$.

3. Experimental Procedures

a. Chemical Search. To determine the energy needed to produce a nuclide by bombarding a target with a projectile, it is necessary to calculate the Q value for the nuclear reaction of interest. The Q value is the mass difference between the reactants and the products of a nuclear reaction. For the reactions involved in this experiment, the mass of the products is greater than the mass of the reactants and the Q value is negative. Energy must be supplied to the projectile to make up this mass difference. The energy required to make a reaction energetically possible is called the "threshold energy," which is the Q value modified by a kinematic factor. For the reactions considered here, the Q value and threshold are approximately the same. The mass predictions of all nuclei with which we are concerned have been calculated by M. Hillman[37] using a semi-empirical mass equation.

Because of the favorable Q values with ^{3}He ions on the cyclotron, a ^{90}Zr target was chosen to make ^{89}Mo:

$$^{90}_{40}Zr_{50} + {}^{3}_{2}He \rightarrow {}^{89}_{42}Mo_{47} + 4n + Q \quad (Q = -30.3 \text{ MeV.})$$

Experimentally, it has been found that the cross section for most reactions in this mass region is largest at the threshold energy for the reaction in which one more neutron is removed. Therefore, to make the maximum amount of ^{89}Mo the target was bombarded near the threshold of the reaction to produce ^{88}Mo.

$$^{90}_{40}Zr_{50} + {}^{3}_{2}He \rightarrow {}^{88}_{42}Mo_{46} + 5n + Q \quad (Q = -37.5 \text{ MeV}).$$

Preliminary experiments were performed by bombarding zirconium oxide (97.8 per cent enriched in ^{90}Zr) with ^{3}He ions of 75, 52 and 40 MeV. The targets were counted 10 min after bombardment. At 75 and 52 MeV, gamma rays from the following isotopes were observed: ^{90}Mo, ^{88}Nb, ^{89}Nb, ^{90}Nb, ^{89}Zr, ^{88}Zr, ^{87}Zr, and ^{86}Zr. A new gamma ray was observed at 204 keV, which had a half-life of 40 min. This was later tentatively identified as a gamma ray from ^{85}Zr. No growth was observed for the 588-keV or 1627-keV gamma rays. At 40 MeV, gamma rays from ^{90}Mo, ^{90}Nb, and ^{89}Zr were observed, but no new gamma radiation was observed.

In order to see weak molybdenum gamma rays which might have been masked by niobium and zirconium radiations, the experiment was repeated with rapid molybdenum chemistry described in Procedure 1 of Chapter II. A target of 66 mg of isotopically enriched zirconium oxide was irradiated with 56 MeV ^{3}He ions for 20 minutes. The sample was counted 17 minutes after bombardment. The only activity observed was from ^{90}Mo. The ^{89}Mo must have decayed very rapidly so that, by the time chemistry was performed to remove niobium, there was no ^{89}Mo remaining. An upper limit for the half-life of $^{89}Mo^{m}$ was determined as 1.75 min and of ^{89}Mo as 27.2 min. To establish a more satisfactory upper limit, the following assumptions were made:

1. There was as much ^{89}Mo and $^{89}Mo^{m}$ made as ^{90}Mo. Therefore, by determining the number of ^{90}Mo nuclei at the end of bombardment one can estimate the number of ^{89}Mo nuclei produced.
2. All niobium was removed by the chemistry.

3. The upper limit for the area of a peak is twice the standard deviation of the background continuum, which consists mostly of Compton events.

4. The growth of the ^{89}Nb peaks is instantaneous.

In actual fact one would expect to produce more ^{89}Mo and ^{89}Mo^{m} than ^{90}Mo at the bombarding energies used in these experiments, since the cross section for a reaction drops as it becomes energetically possible to make other isotopes. However, since no one has actually measured the excitation functions for these reactions it is difficult to determine just how much more ^{89}Mo or ^{89}Mo^{m} is being made. Yet, to establish an upper limit it is safe to assume that the total yield of ^{89}Mo and ^{89}Mo^{m} was the same as the yield of ^{90}Mo.

In no experiment will all the niobium be removed. Tracer experiments have shown that the decontamination factor for niobium and technetium is about 100 and 200, respectively. The decontamination factor is defined as the amount of activity present before chemistry divided by the amount of activity present after chemistry, multiplied by the percentage yield of the element being assayed, in this case, molybednum. These factors are relatively low, but the niobium cross section is about a factor of five lower than molybdenum for the conditions used in the experiment. The technetium activity produced was short-lived, and most of it decayed away before chemistry was performed.

Generally it is assumed that a peak with an area less than twice the statistical deviation in background cannot be treated as valid. In many of the preceding experiments no peak was seen at the energies corresponding to 588 keV or 1627 keV.

In an equation of growth and decay the time (t_{max}) for the daughter activity to reach its maximum is determined from the following equation:

$$t_{max} = \left(\frac{1}{\lambda_2 - \lambda_1}\right) \frac{\lambda_2}{\lambda_1} .$$

The decay constant of ^{89}Mo λ_1 is much greater than the decay constant of ^{89}Nb λ_2. Therefore, the value of t_{max} will be very small. Usually, the limit of peak area for ^{89}Nb or $^{89}Nb^m$ was taken after several hours of counting. When correcting for the decay from time t_{max}, one can safely correct to the time of the end of bombardment or to the end of the niobium chemistry, since t_{max} is so small. The ^{90}Mo gamma ray at 257 keV was used to calculate the amount of ^{90}Mo, and consequently ^{89}Mo, present.

To determine the number of nuclei present from the area of the peak P_γ, one must divide by the efficiency of the detector ε and relative intensity of the gamma ray I_γ. The decay rate is designated as λ, and N represents the number of nuclei formed.

$$A = \frac{P_\gamma}{\varepsilon I_\gamma} ,$$

and

$$N = \frac{A}{\lambda} = \frac{P}{\lambda \varepsilon I_\gamma} .$$

The activity A must be corrected for decay from time t_{max}.

The ^{89}Nb counted after niobium was chemically separated must be assumed to have been formed from the decay of ^{89}Mo. Therefore, by knowing the number of nuclei of ^{89}Mo present at two different times a half-life can be estimated:

$$\frac{A_o}{A} = e^{\lambda t} = e^{\frac{.693}{t_{max}} t}$$

$$t_{max} = \left(\frac{1}{.693t}\right) \ln \frac{A_o}{A}$$

The activity of ^{90}Mo at the end of bombardment provides the information for A_o, since the number of nuclei produced is proportional to the activity as shown in the equation below

$$A_o = N\lambda$$

where λ is the decay constant for ^{90}Mo. The amount of niobium formed after chemistry represents A. The time interval, t, is the time between the end of the bombardment and the end of the niobium chemistry. In this way an upper limit was obtained for the half-life.

One of the slow steps in the previous chemistry procedure was the dissolution of the zirconium oxide target. To increase the speed of chemistry, proton irradiations were made on targets of potassium niobate, which quickly dissolves in water. Since protons are degraded less than helium ions by the target, a more massive target could be used and the activity increased. Procedure 2 of the molybdenum separations in Chapter II was used for the chemical separation. A target of 222 mg of potassium niobate was irradiated with 63-MeV protons. The sample was then counted 13 min after bombardment. Only ^{90}Mo activity was observed. An upper limit of 1.35 min was set for the half-life of $^{89}Mo^{m}$, and an upper limit of 1.5 min was set for ^{89}Mo.

Additional experiments were performed on ^{92}Mo foil with a thickness of 100 mg cm^{-2}. The target was bombarded with protons in a

vacuum-tight scattering chamber. A detector was set up nearby, so that the target could be counted immediately after the beam was cut off. The Q value for the $^{92}Mo(p,p3n)^{89}Mo$ reaction is 34.5 MeV. Bombardments were made at energies of 40.0 MeV, 56.3 MeV and 31.0 MeV. Bombardments were made for ca. 60 sec and the target was counted 20 sec after each bombardment. At 40 MeV and 56.3 MeV, gamma rays were seen from 4.1-min ^{92}Tc, 1.6-min $^{91}Mo^{m}$, 5.7-hr ^{90}Mo, 66-min $^{89}Nb^{m}$, and 14-min ^{88}Nb. At 31.0 MeV only ^{92}Tc, $^{91}Mo^{m}$ and ^{90}Mo were seen. The Q value for the $^{92}Mo(p,2p2n)^{89}Nb$ reaction is 33 MeV. The Q value for the $^{92}Mo(p,2p3n)^{88}Nb$ reaction is 47 MeV. From these calculations it can be seen that ^{89}Nb and ^{88}Nb could have been made directly. No growth was seen for $^{89}Nb^{m}$ and ^{88}Nb, although it was difficult to set very low limits, since the peaks of interest lay in a region of intense Compton background from other gamma rays. Chemistry then was necessary before any weak peaks could be observed. It was evident that the time interval between the end of bombardment and the counting time must be reduced. Therefore, a chemical separation apparatus was set up on the end of the beam pipe. Remote controls were used so that chemical steps could be performed while the door to the experimental room was being opened. A television monitor allowed the operator to see the various chemistry steps. Procedure 3 was used for this type of experiment, as described earlier in Chapter II.

Bombardments were made at 41 MeV, 57 MeV, and 63 MeV. In all experiments only the gamma rays characteristic of 1.6-min $^{91}Mo^{m}$ and 5.7-hr ^{90}Mo were observed. The upper limits for these half-lives are shown in Table VIII.

TABLE VIII

SUMMARY OF THE UPPER LIMITS FOR ^{89}Mo AND $^{89}Mo^{m}$ HALF-LIVES DETERMINED FROM THE FOUR DIFFERENT CHEMICAL PROCEDURES

Procedure	Projectile	Energy (MeV)	Target	Upper Limit for $^{89}Mo^{m}$	Upper Limit for ^{89}Mo
1	^{3}He	56	$^{90}ZrO_2$	1.75 min	27.2 min
2	H	63	K_3NbO_4	1.35 min	1.5 min
3	H	41	$^{92}Mo^{6+}$	30 sec	X[a]
3	H	57	$^{92}Mo^{6+}$	28 sec	1.6 min
3	H	63	$^{92}Mo^{6+}$	38 sec	1.3 min
4	H	62	^{92}Mo	24 sec	43 sec

[a]Sample was not counted for a long enough time to obtain a meaningful upper limit.

Most of the activity seen in these experiments was due to positron annihilation radiation. It was suspected that much of this activity was from 124-sec ^{15}O produced in the $^{16}O(p,pn)^{15}O$ reaction. The oxygen in the molybdate ion must have become radioactive and would have been carried on the α-benzoin oxime precipitate.

To eliminate this problem, metallic ^{92}Mo was irradiated in a test tube, and Procedure 4 was used to separate molybdenum activity from all others. A picture of the apparatus was shown earlier in Figures 7 (p.41) and 8 (p.42). About 10 mg of metallic ^{92}Mo was bombarded with 61-MeV protons for about one min. Chemistry was successfully performed, and the sample was counted 5 min after bombardment. Again, the only gamma rays seen were from 1.5-min $^{91}Mo^{m}$ and 5.7-hr ^{90}Mo. The half-life lower limit from this experiment was 24 sec for $^{89}Mo^{m}$ and 43 sec for ^{89}Mo.

b. Excitation Function. It is possible that ^{89}Mo was not even being made. Although it is unlikely, one might speculate that the nuclear structure in this mass region is sufficiently different that the calculated masses are grossly in error. To confirm that ^{89}Mo was indeed being made, an experiment was performed to infer an excitation function for ^{90}Mo. Since normal reaction cross sections decrease when other reactions become energetically possible and begin to compete, the cross section for ^{90}Mo will decrease when it becomes possible to make ^{89}Mo.

Five ^{92}Mo targets were prepared with various amounts of degrading foil between them, so that the beam energy changed as it traveled through the target and degrading foil stack. The activity per milligram was

determined by counting the strong 257-keV gamma ray of ^{90}Mo. The excitation function obtained from these results is shown in Figure 20. The drop beyond the peak of the function shows that production of ^{89}Mo should begin at about 45 MeV. This would suggest that ^{89}Mo was made at energies greater than 45 MeV.

The ^{90}Zr nucleus is very similar to ^{92}Mo. By bombarding ^{90}Zr with 62 MeV protons and observing the products, one should be able to predict the corresponding amounts of ^{92}Mo products. A 10-mg target of zirconium oxide (97.8 per cent enriched in ^{90}Zr) was bombarded with 62-MeV protons for 15 min. The chemical separation for zirconium was described in Chapter II. Gamma rays from ^{89}Zr, ^{88}Zr, and ^{86}Zr were observed. Also, several gamma rays were observed to decay with a 40-min half life. These may have been from ^{85}Zr, whose decay has not been well studied.

As far as is presently known, ^{87}Zr does not emit any gamma rays in its decay, but it decays to ^{87}Y^{m}, which emits a 381-keV gamma ray. The amount of ^{87}Y^{m} present corresponds to the amount of ^{87}Zr produced in the bombardments. Table IX indicates the relative amounts of each zirconium isotope determined in the bombardment of ^{90}Zr with 62-MeV protons.

The ^{90}Zr(p,p3n)^{87}Zr reaction corresponds to ^{92}Mo(p,p3n)^{89}Mo reaction. Table IX shows ^{87}Zr was made in large amounts and suggests that not only ^{89}Mo but also ^{88}Mo and ^{87}Mo should have been made in large quantities.

c. Final Results. It is energetically possible that ^{89}Mo could

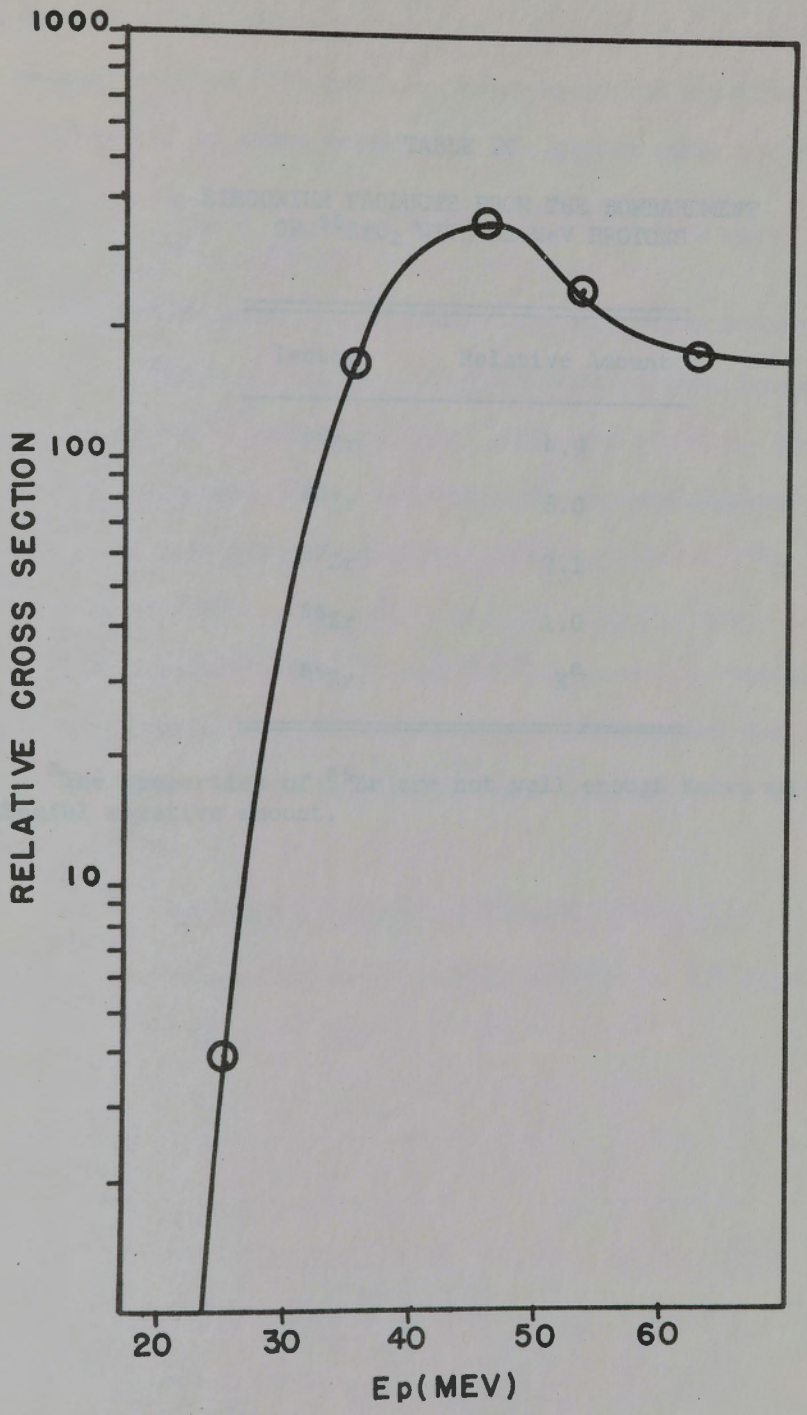


Figure 20. Excitation function for $^{92}Mo(p,p2n)^{90}Mo$.

TABLE IX

ZIRCONIUM PRODUCTS FROM THE BOMBARDMENT OF $^{90}ZrO_2$ WITH 62-MeV PROTONS

Isotope	Relative Amount
^{89}Zr	4.9
^{88}Zr	6.0
^{87}Zr	7.1
^{86}Zr	1.0
^{85}Zr	X[a]

[a]The properties of ^{85}Zr are not well enough known to obtain a meaningful relative amount.

be a delayed proton emitter. That is, it could beta decay to a very high energy level of ^{89}Nb and then decay by proton emission to form ^{88}Zr, instead of by gamma emission to the ground state of ^{89}Nb:

$$^{89}_{42}\mathrm{Mo} \rightarrow {}^{88}_{40}\mathrm{Zr} + p^{+} + \beta^{+} + Q \qquad (Q = 2.04 \text{ MeV})$$

To search for ^{88}Zr a target was counted 76 days after bombardment (the half-life of ^{88}Zr is 85 days). All other activity had decayed, so only the background would mask the 393-keV gamma ray of ^{88}Zr. The sample was counted for a day, but no 393-keV gamma ray was observed. This result made it possible to set an upper limit of 1.2 min for the delayed-proton decay of ^{89}Mo.

It is possible that ^{89}Mo and ^{89}Mo^{m} isomers are very long lived, so that very little ^{89}Nb would be formed. If this were the case, secular equilibrium would be attained, and the activity of ^{89}Nb would be the same as ^{89}Mo:

$$N\,(^{89}\mathrm{Mo})\,\lambda\,(^{89}\mathrm{Mo}) = N\,(^{89}\mathrm{Nb})\,\lambda\,(^{89}\mathrm{Nb})\ .$$

The lower limit calculated for the decay of ^{89}Mo is 4.6 days.

CHAPTER IV

CONCLUSION

The spins and parities of the first few excited states of ^{89}Y that were found experimentally are in good agreement with predictions. The $9/2^+$ excited state corresponds to the last proton excited to the $g_{9/2}$ shell. The $3/2^-$ state at 1507.4 keV corresponds to a $3/2^-$ proton coupling with the $1/2^-$ proton, so that the remaining $3/2^-$ hole determines the spin. Likewise, the $5/2^-$ state corresponds to the coupling of a $5/2^-$ proton with the $1/2^-$ proton, leaving a $5/2^-$ hole. The $5/2^+$ state at 2.222 MeV which was not observed from beta decay may represent the proton in a $d_{5/2}$ state. Likewise, the $7/2^+$ state may represent the proton excited to the $g_{7/2}$ state. Other excited states would represent excited neutron pairs with spins of 0^+, 2^+, 4^+ and 6^+ coupling with the proton holes.

The log *ft* values for the allowed transitions between the $9/2^+$ states and the $1/2^-$ states are larger than usual. This is because only a fraction of the ^{89}Zr nuclei have their proton pairs in the $p_{1/2}$ levels; the remaining available protons are in the $g_{9/2}$ level. Beta transitions to the $1/2^-$ ground state of ^{89}Y require a $p_{1/2}$ proton to decay to a neutron. Since only a small fraction of $p_{1/2}$ protons are available, such beta transitions are hindered. In a similar manner the $9/2^+ \rightarrow 9/2^+$ transition is hindered, but to a lesser degree, since in some cases the last two protons do not fill the $g_{9/2}$ shell.

The excited states in ^{89}Zr are very similar in nature to the

excited states of ^{89}Y. Here, the neutron holes are the dominant feature of the properties of the nuclear states. The $1/2^-$ level at 588 keV represents the neutron hole made when the $p_{1/2}$ neutron couples to the $9/2^+$ neutron in the $g_{9/2}$ shell. Likewise, the 1096-keV and 1451-keV levels correspond to $3/2^-$ and $5/2^-$ neutron holes. The 1512-keV level identified as $9/2^+$ from reaction work corresponds to a proton pair excited to the $5/2^+$ level. Since they remain coupled, they contribute nothing to the spin, which is determined by the $g_{9/2}$ neutron. The lone neutron excited to the $5/2^+$ state probably represents the $5/2^+$ state observed at 1627 keV. Other spins represent 0^+, 2^+, 4^+ and 6^+ couplings of the proton pairs with neutron holes of spins $1/2^-$, $3/2^-$, and $5/2^-$.

This dissertation has shown that the half-life of ^{89}Mo is either shorter or much longer than that determined by Butement. The high-energy beta rays measured in his work may correspond to beta rays of ^{91}Mo. The half-life is a factor of two different than the half-life of ^{91}Mo measured by other experimenters; however, his work on ^{88}Nb and ^{89}Nb isotope half-lives has been shown to be incorrect by almost a factor of two,[38,39] or he may have measured the random counts from ^{91}Mo.

The half-life of $^{91}Mo^m$ was measured as 66 sec. It is not unlikely that the half-life of an isomer two neutrons removed from $^{91}Mo^m$ and further removed from the stability region would have a half-life less than 24 seconds. In a similar manner, a 43-sec half-life is feasible for ^{89}Mo, which is two neutrons removed from 15 min ^{91}Mo.

The same method can be used to determine an upper limit for the

half-life of ^{88}Mo as was used to determine the upper limit on the half-life of $^{89}Mo^{m}$, since ^{88}Nb has a 627-keV gamma ray which has a relative intensity and detector efficiency almost the same as the 588-keV gamma ray of $^{89}Nb^{m}$. In this way, an upper limit on the half-life of ^{88}Mo of 24 sec was established. Since the ^{89}Mo excitation function cannot be determined, it is not certain that ^{88}Mo was made at proton energies less than 63 MeV, although the result shown in Table IX (p. 96) would suggest that it could be made. A half-life of less than 24 sec seems abnormally short for ^{88}Mo, since ^{90}Mo has a half-life of 5.7 hr. Perhaps this is a region of sharply increasing instability with decreasing mass number, which suggests profitable, fascinating research for the future.

Archives
esis
9b
333

BIBLIOGRAPHY

Archives
esis
96
833

BIBLIOGRAPHY

1. M. G. Mayer and J. Hans D. Jensen, "Elementary Theory of Nuclear Shell Structure," John Wiley and Sons, New York, N. Y., 1955, Chapter 4.

2. S. G. Nilsson, Dan. Mat-fys. Medd, 29, No. 16 (1955).

3. G. E. Gorden and C. D. Coryell, J. Chem. Ed., 44, 636 (1967).

4. R. D. Woods and D. S. Saxon, Phys. Rev., 95, 577 (1954).

5. L. W. Nordheim, Phys. Rev., 78, 322 (1951).

6. M. H. Brennan and A. M. Bernstein, Phys. Rev., 120, 927 (1960).

7. M. Goldhaber, Phys. Rev., 89, 1146 (1953).

8. I. Talmi, Rev. Mod. Phys., 34, 704 (1962).

9. K. H. Bhatt and J. B. Ball, Nucl. Phys., 63, 286 (1965).

10. J. Vervier, Nucl. Phys., 75, 17 (1966).

11. I. Talmi and I. Unna, Nucl. Phys., 19, 225 (1960).

12. S. A. Moszkowski in "Alpha-Beta, and Gamma-Ray Spectroscopy," Vol. 2, K. Siegbahn, Ed., North Holland Publishing Company, Amsterdam, 1965, Chapter 23.

13. E. Fermi, Z. Phys., 88, 161 (1934).

14. E. J. Konopinski and M. E. Rose, in "Alpha-, Beta- and Gamma-Ray Spectroscopy," Vol. 2, K. Siegbahn, Ed., North Holland Publishing Company, Amsterdam, 1965, Chapter 23.

15. F. N. D. Kurie, J. Richardson, and H. Paxton, Phys. Rev., 49, 368 (1939).

16. G. Friedlander, J. Kennedy, J. Miller, "Nuclear and Radiochemistry," 2nd ed., John Wiley and Sons, New York, N. Y., 1964, pp. 138-139.

17. G. D. O'Kelley, "Detection and Measurement of Nuclear Radiation," National Academy of Sciences-National Research Council, Report NAS-NS 3105, Washington, D. C., 1962, pp. 59-65.

18. D. C. Camp, "Applications and Optimization of the Lithium-Drifted Germanium Detector System," University of California, Report UCRL-50156, Livermore, Calif., 1967, pp. 126-127.

19. A. Jenkins, unpublished program, Oak Ridge National Laboratory, Oak Ridge, Tenn., 1966.

20. R. C. Hagenauer, unpublished program, Oak Ridge National Laboratory, Oak Ridge, Tenn., 1968.

21. R. A. Kuebbing, unpublished program, Oak Ridge National Laboratory, Oak Ridge, Tenn., 1968.

22. P. C. Rogers, Massachusetts Institute of Technology, Report NYO-2303, Cambridge, Mass., 1962.

23. D. M. Van Patter and S. M. Shafroth, Nucl. Phys., 50, 113, (1964).

24. P. F. Hinrichsen, Nucl. Phys., A118, 538 (1968).

25. C. P. Swann and F. R. Metzger, Phys. Rev., 82, 944, (1951).

26. J. H. Hamilton, L. M. Langer, and W. C. Smith, Phys. Rev., 119, 772 (1960).

27. P. F. Hinrichsen, S. M. Shafroth, and D. M. Van Patter, Nucl. Phys., 172, 1134 (1968).

28. P. S. Buchanan, S. C. Mathur, W. E. Tucker, and J. L. Morgan, Phys. Rev., 158, 1041 (1967).

29. R. M. Diamond, Phys. Rev., 95, 410 (1954).

30. H. B. Mathur, E. K. Hyde, C. A. Levine, and P. K. Kafstad, Phys. Rev., 97, 117 (1955).

31. E. K. Hyde and J. M. Nitschke, University of California Radiation Laboratory, Report UCRL-16580, Berkeley, Calif., 1966.

32. A. Hanser and J. Flegenheimer, Radiochim. Acta, 5, 120 (1966).

33. J. B. Ball and C. B. Fulmer, Phys. Rev., 172, 1199 (1968).

34. H. Taketani, M. Adachi, Y. Yoshida, M. Ogawa, and K. Ashibe, Phys. Lett., 27B, 499 (1968).

35. J. B. Ball, Oak Ridge National Laboratory, personal communication, 1968.

36. F. D. S. Butement and S. M. Qaim, J. Inorg. Nucl. Chem., 26, 1491 (1964).

37. M. Hillman, Brookhaven National Laboratory, Report T-333, Upton, New York, March, 1964.

38. F. D. S. Butement and S. M. Qaim, J. Inorg. Nucl. Chem., 26, 1481 (1964).

39. J. Flegenheimer, Radiochim. Acta., 6, 20 (1966).

40. J. A. Harvey, M. M. Stevens, Oak Ridge National Laboratory, Report ORNL-4082, Oak Ridge, Tenn., May, 1967.

Archives
esis
9b
333

APPENDIX

Archives
Thesis
96
233

APPENDIX

PROGRAM DAZYMA

Program DAZYMA was written to analyze a large number of gamma-ray spectra for peak areas, energies, and half-lives. For input it uses data written on magnetic tape, which in turn may have been converted from paper tape recorded on the Victoreen SCIPP 16-channel analyzer, or from primary magnetic tapes produced by the Victoreen 20,000-channel analyzer. DAZYMA combines the locally-used GRAP[40] program for peak fitting and FRANTIC for growth and decay analysis.

Initially, the number of counts for each channel is read from the magnetic tape into an array stored in the computer memory. The peak-finding subroutine, PKFIND, tests the counts in each channel, y(a), to see if the number is statiscally greater than that of the previous channel. That is,

$$y(a + 1) = y(a) + \sqrt{y(a)}.$$

If not, the program advances to the next channel. If the channel value statistically exceeds the value at the previous point, the program considers the channel a possible peak location and conducts other tests. Once the peak channel is determined, the program tests to be certain it is not a spurious peak due to an analyzer malfunction. Another test determines a background on each side of the peak. If the average of the three largest counts in the peak is not 2.2 times the standard deviation of the background, the program disregards it and continues to look for

another possible peak. If it passes this test, a centroid guess (cent.) is made by determining a weighted average:

$$\text{cent.} = \sum_{1}^{5} \frac{N(Y) \times Y}{\sum_{1}^{5} Y},$$

where N(Y) is the number of counts in channel Y. The five highest counts in the peak are used for this determination. These centroids are stored in the memory to be used as initial guesses for subroutine GRAP.

Since GRAP can analyze several peaks at once, subroutine PREGRA divides the spectra into blocks which contain groups of peaks close together. A provision is made to exclude very weak peaks near peaks of high intensity. Each block of peaks is then analyzed by subroutine GRAP, which fits a baseline to the points making up the background of the peaks. The corresponding background value is subtracted from each point in the peak. The peak is then fitted to a function of the form

$$y = 4h \left[e^{-(x-x_o)/s(1+\alpha)} + e^{(x-x_o)/s(1-\alpha)} \right]^{-2},$$

where x_o is the value of the center, h is the height, s is the width and α is an assymmetry parameter, used when peaks are skewed. Unless indicated otherwise, the program assumes the peaks are not skewed, and makes α equal to zero. The equation then reduces to the form:

$$y = h \operatorname{sech}^2 [x-x_o)/s]$$

This equation is very similar to a Gaussian. Parameter guesses x_o and h are calculated in subroutine PKFIND. The s value used is the same one used by the previous peak, since the width changes only slightly with

Archives
Thesis
C96
S33

energy. These parameter guesses are varied until the differences between the calculated y values and the data y values reach a minimum. The area is then calculated from the height, asymmetry and width parameters.

$$\text{Area} = 2hs(1-\alpha^2)\ \frac{\pi\alpha}{\sin\ \pi\alpha}$$

Once the position is determined, the energy can be calculated from a calibration which has been read from cards or from a calibration spectrum on magnetic tape. If DAZYMA read a calibration spectrum into the memory, it finds all the peak positions and areas and arranges the peaks by intensity. The most intense peaks are then assigned an energy from a calibration library compiled as part of the program. A code number identifies the position in the calibration library where the energies correspond to the intense peaks. Several spectra may be used for calibration. The calibration energies and channels are then ordered by energy, and the slope of the calibration curve in keV/channel is then calculated for each region of the spectrum.

Once the position of the analyzed peak is determined, the program searches for the region where the peak position will be between two calibration points. After determining which of the two calibration points is closer, the difference in channel position between the peak and calibration point is multiplied by the calibration slope in keV/channel. The energy difference is then added or subtracted from the right or left calibration point as shown below:

$$\Delta Ch = P - C$$

$$\Delta E = \Delta Ch \times \text{keV/channel}$$

$$E = E_{cal} + \Delta E$$

Archives
Thesis
C96
S33

where ΔCh is the channel difference between the peak position (P) and channel position of the calibration point (C), ΔE is the energy difference between the calibration energy (E_{cal}) and the energy of the peak in question (E).

The energy, position, area, counting time, and starting time are then placed in a storage array. After the area of each peak is found, the program inspects the computer memory for a peak of the same channel position from another spectrum. If one is found, the area value, time interval, and starting time are then added to that array. If not, a new array is started.

After all peaks are analyzed for area, half-life determinations can be made. For this analysis, DAZYMA used the FRANTIC part of the program. For each peak the information such as area, time interval, and counting time is ordered according to starting time. The data then are analyzed for half-life in the normal FRANTIC method, assuming one-component decay. The program guesses a half-life from the first and last data points and iterates around this guess until a half-life is obtained from a least squares method. If the fit is poor and there are five or more data points, DAZYMA tries to fit two components to the data. After each fit, the results are printed in the normal FRANTIC output. In this way the experimenter can compare the results of the two fits. This process is completed for each set of peaks.

Finally, the program summarizes the data in five parts: decaying peaks, growing peaks, two-component peaks, peaks with matrix inversion problems, and peaks which occurred in only one spectrum. The growing

Archives
Lesis
596
233

and decaying peaks are ordered by half-life. The channel position, half-life, standard deviation, A_o, and energy are printed in tabular form. Thus, if the spectra contain nuclides of different half-life, the experimenter can easily sort out the gamma rays characteristic of that isotope from the half-life. Peaks occurring in only one spectrum are either short-lived or spurious peaks found by subroutine PKFIND.

Archives
Thesis
G9b
W33

VITA

Richard Carl Hagenauer was born in New York City on June 27, 1942. He was raised and educated in the elementary schools near Freeport, Pennsylvania. In May, 1960 he was graduated from Freeport High School. The following September he entered Wheaton College in Illinois and was graduated in June, 1964 with a Bachelor of Science degree. In September, 1964 he entered the Graduate School of the University of Tennessee, holding a teaching assistantship. In June, 1966 he received a fellowship from Oak Ridge Associated Universities enabling him to work at Oak Ridge National Laboratory, Oak Ridge, Tennessee.

Mr. Hagenauer is married to Emily Carol Moore Hagenauer of Bridgeton, New Jersey. They have one son, Gary Scott.